PARK7/DJ-1 deficiency impairs microglial activation in response to LPS-induced inflammation

Frida Lind-Holm Mogensen
Luxembourg Institute of Health
Carole Sousa
Luxembourg Institute of Health
Corrado Ameli
University of Luxembourg
Katja Badanjak
University of Luxembourg
Arnaud Muller
Luxembourg Institute of Health
Tony Kaoma
Luxembourg Institute of Health
Djalil Coowar
University of Luxembourg
Andrea Scafidi
Luxembourg Institute of Health
Suresh K Poovathingal
University of Luxembourg
Nathalie Nicot
Luxembourg Institute of Health & Laboratoire National de Santé
Aurélien Ginolhac
University of Luxembourg
Daniela M Vogt Weisenhorn
Helmholtz Zentrum München-German Research Center for Environmental Health
Wolfgang Wurst
Helmholtz Zentrum München-German Research Center for Environmental Health
Aurélie Poli
Luxembourg Institute of Health
Petr V Nazarov
Luxembourg Institute of Health
Alexander Skupin
University of Luxembourg
Anne Grünewald

University of Luxembourg
Alessandro Michelucci (alessandro.michelucci@lih.lu)
Luxembourg Institute of Health

Research Article

Keywords: PARK7/DJ-1, Lipopolysaccharide, Microglia, Neuroinflammation, Parkinson's disease, Microglia morphology

Posted Date: February 9th, 2024

DOI: https://doi.org/10.21203/rs.3.rs-3931138/v1

Additional Declarations: No competing interests reported.

Abstract

Background

Specific microglia responses are thought to contribute to the development and progression of neurodegenerative diseases, including Parkinson's disease (PD). However, the phenotypic acquisition of microglial cells and their role during the underlying neuroinflammatory processes remain largely elusive. Here, according to the multiple-hit hypothesis, which stipulates that PD etiology is determined by a combination of genetics and various environmental risk factors, we investigate microglial transcriptional programs and morphological adaptations under *PARK7*/DJ-1 deficiency, a genetic cause of PD, during lipopolysaccharide (LPS)-induced inflammation.

Methods

Using a combination of single-cell RNA-sequencing, bulk RNA-sequencing, multicolor flow cytometry and immunofluorescence analyses, we comprehensively compared microglial cell phenotypic characteristics in *PARK7*/DJ-1 knock-out (KO) with wildtype littermate mice following 6- or 24-hour intraperitoneal injection with LPS. For translational perspectives, we conducted corresponding analyses in human *PARK7*/DJ-1 mutant induced pluripotent stem cell (iPSC)-derived microglia and murine bone marrow-derived macrophages (BMDMs).

Results

By excluding the contribution of other immune brain resident and peripheral cells, we show that microglia acutely isolated from *PARK7*/DJ-1 KO mice display a distinct phenotype, specially related to type II interferon and DNA damage response signaling, when compared with wildtype microglia, in response to LPS. We also detected discrete signatures in human *PARK7*/DJ-1 mutant iPSC-derived microglia and BMDMs from *PARK7*/DJ-1 KO mice. These specific transcriptional signatures were reflected at the morphological level, with microglia in LPS-treated *PARK7*/DJ-1 KO mice showing a less amoeboid cell shape compared to wildtype mice, both at 6 and 24 hours after acute inflammation, as also observed in BMDMs.

Conclusions

Taken together, our results show that, under inflammatory conditions, *PARK7*/DJ-1 deficiency skews microglia towards a distinct phenotype characterized by downregulation of genes involved in type II interferon signaling and a less prominent amoeboid morphology compared to wildtype microglia. These findings suggest that the underlying oxidative stress associated with the lack of *PARK7*/DJ-1 affects microglia neuroinflammatory responses, which may play a causative role in PD onset and progression.

Background

Microglia serve as the central nervous system's primary immune effector cells. Under threatening conditions, microglia rapidly react by undergoing transcriptional, morphological and functional changes, known as "microglia activation". This process encompasses various stages and substates, which vary depending on the context and duration of the compromising conditions, seeking to resolve the threat efficiently (Paolicelli, Sierra et al. 2022).

Parkinson's disease (PD) is the second most common neurodegenerative disease, which involves the accumulation of α-synuclein and the progressive loss of dopaminergic neurons. The main risk factor for PD is aging and, as the world´s population becomes older, the number of people diagnosed with a neurodegenerative disease continues to increase (Dorsey, Sherer et al. 2018). Additionally, factors beyond aging, such as pesticide exposure and infections, may contribute significantly to this trend, as the incidence of PD currently outpaces the rate of aging and is disproportionally on the rise, a tendency that is particularly noticeable in newly industrialized countries (Dorsey, Sherer et al. 2018). The notion that PD is caused by a combination of genetics and different environmental risk factors refers to the multiple-hit hypothesis (Patrick, Bell et al. 2019). Among the detected genetic defects, the loss of function of *PARK7*, encoding for the protein DJ-1, causes autosomal recessive early-onset PD in humans. DJ-1 is a multifunctional protein with roles in cellular transformation, transcriptional regulation, and anti-oxidative stress functions (Clements, McNally et al. 2006). On the other hand, a number of bacterial and viral infections, including *Helicobacter pylori* (Nielsen, Qiu et al. 2012, Bu, Wang et al. 2015) and hepatitis C virus (Pakpoor, Noyce et al. 2017), have been linked to increased idiopathic PD risk, thus indicating a potential contributing role of infections in the development or exacerbation of the disease, at least in certain individuals (Fang, Wirdefeldt et al. 2012, Wang, Liu et al. 2020, Smeyne, Noyce et al. 2021).

Activated microglial phenotypes and neuroinflammatory processes are detected in the early stages of PD and in the *substantia nigra* of post-mortem tissues (Imamura, Hishikawa et al. 2003, Gerhard, Pavese et al. 2006, Lavisse, Goutal et al. 2021, Smajic, Prada-Medina et al. 2022). However, the role of microglia in the onset and progression of PD remains vague. In line with the multi-hit hypothesis, we here postulate that *PARK7*/DJ-1 deficiency influences microglial responses under inflammatory conditions. To address this hypothesis, we took advantage of the *PARK7*/DJ-1 KO mouse model, which shows subtle impairments in cognitive and motor functions and heightened vulnerability to neurotoxins (Chen, Cagniard et al. 2005, Goldberg, Pisani et al. 2005, Kim, Smith et al. 2005). How microglia react in those mice under inflammatory conditions has not been thoroughly addressed as most of the studies have been conducted *in vitro* using *PARK7*/DJ-1 deficient immortalized microglial cell lines, which show an exacerbated response to inflammatory stimuli (Lind-Holm Mogensen, Scafidi et al. 2023). By comparing the transcriptional profile of sorted microglial cells isolated from *PARK7*/DJ-1 KO with wildtype mice peripherally injected with lipopolysaccharide (LPS), a stimulus we have previously shown to induce a prominent microglia activation (Sousa, Golebiewska et al. 2018), we identified distinct signatures of this activated state. Specifically, microglia in *PARK7*/DJ-1 KO LPS-treated mice were characterized by the downregulation of genes involved in immune responses, especially interferon-related genes, and

upregulation of genes related to DNA damage response, when compared to the corresponding cells isolated from wildtype mice. We further confirmed a dampened transcriptional response towards LPS in human *PARK7*/DJ-1 mutant compared to isogenic control induced pluripotent stem cell (iPSC)-derived microglia and murine bone marrow-derived macrophages. Furthermore, in line with these distinct profiles detected at the transcriptional level, microglial cells in *PARK7*/DJ-1 KO mice exhibited a less prominent amoeboid shape, indicating a less reactive phenotype, when compared to wildtype mice in response to LPS-induced systemic inflammation.

Taken together, our results show that, under inflammatory conditions, *PARK7*/DJ-1 deficiency skews microglia towards a distinct phenotype, which may have an impact during neuroinflammatory processes under threatening conditions, such as during α-synuclein accumulation at the onset and during the progression of PD.

Materials and Methods

Mice

PARK7/DJ-1 KO (B6;129P2-*Park7*$^{Gt(XE726)Byg}$/Mmucd) mice were kindly provided by the laboratory of Dr D.M. Vogt Weisenhorn in Munich (Germany), where they have been originally developed and characterized (Pham, Giesert et al. 2010). The *PARK7*/DJ-1 KO line used in our laboratory had already been backcrossed with C57BL/6NCrl mice for at least ten generations. For all the described experiments, except for the single-cell RNA-sequencing experiments where each condition was analyzed by mixing cells from one male and one female, we used male *PARK7*/DJ-1 KO and wildtype littermate mice that were 3- and 4-month age-matched siblings generated from heterozygous breeding pairs. Mice were bred and housed in a specific pathogen-free animal research facility at a relative humidity of 40–70%, at 22°C and in 12 hours light/dark cycles. Mice received food (SAFE A40) and water *ad libitum*.

PARK7 /DJ-1 KO mouse genotyping

PARK7/DJ-1 KO, heterozygote and wildtype littermates were genotyped using a genotyping kit (KAPA Biosystems, KK7352), following the manufacturer's instructions. Briefly, genomic DNA was extracted from mouse ear marking samples or tail pieces. The PCR cycling program (BioRad 3000) was as follows: 1 cycle of initial denaturation at 95°C for 3 minutes followed by 35 cycles of denaturation at 95°C for 15 seconds, annealing at 58°C for 15 seconds and extension at 72°C for 15 seconds, ended by a final extension at 72°C for 7 minutes. Primers used for genotyping were as follows. Wildtype *Park7* forward primer: 5'-AGGCAGTGGAGAAGTCCATC-3'; wildtype *Park7* reverse primer: 5'-AACATACAGACCCGGGATGA-3'; KO *Park7* reverse primer: 5'-CGGTACCAGACTCTCCCATC-3'. PCR products loaded on a 2% agarose gel showed bands at 475bp or 231bp, corresponding to wildtype or KO alleles, respectively.

Acute microglia isolation by fluorescence-activated cell sorting (FACS)

Mice were treated with a single intraperitoneal injection of LPS (4 µg/g body weight) or with PBS (saline) as vehicle control for 24 hours. Processing of the brain, microglial isolation and multicolor flow cytometry preparation was done as previously described (Sousa, Golebiewska et al. 2018). Briefly, myelin was removed from cell suspension with the Myelin removal kit (130-096-733, Miltenyi Biotec), according to the manufacturer's protocol. For multicolor staining, cells were incubated for 15 minutes with Fc receptor binding inhibitor to reduce the binding of non-specific Fc-gamma receptors, and then stained with fluorochrome-conjugated antibodies or their corresponding isotype controls for 45 minutes at 4°C in the dark (**Table S1**). After washing, cells were pelleted at 300 g for 10 minutes at 4°C and resuspended in 200 µL of the appropriated buffer. Hoechst (0.1 µg/ml; Sigma) or Sytox Red (1:1000; Thermo Fisher Scientific) were added shortly before flow cytometry measurements for dead cell discrimination. $CD11b^{+}CD45^{int}$ living single cells were sorted with FACS Aria™ SORP cytometer (BD Biosciences) fitted with a 640 nm (30 mW) red laser, a 355 nm (60 mW) UV laser, a 405 nm (50 mW) violet laser, a 488 nm (100 mW) blue laser and a 561 nm (50 mW) yellow/green laser. Data were analyzed with FACSDiva (Becton Dickinson) and FlowJo (v7.6.5; Tree Star) software.

Single-cell RNA-sequencing using Drop-seq, bioinformatics and data analyses

FACS-sorted $CD11b^{+}CD45^{int}$ cells were collected in pre-cooled HBSS, 0.5% BSA and transferred directly for subsequent Drop-seq analysis as previously described (Sousa, Golebiewska et al. 2018).

Cell calling, normalization and scaling

DropletUtils (Lun, Riesenfeld et al. 2019) was employed to distinguish cells from empty droplets. Subsequently, raw gene counts of the identified "*cells*" were converted into Seurat object (Hao, Hao et al. 2021). Cells expressing less than 100 genes and genes detected in less than 3 cells were discarded. The resulting object was subjected to log-normalization and scaling using the standard functions of the Seurat package (*NormalizeData and ScaleData;* Seurat v4.3.0.1).

Dimension reduction and clustering

Principal component analysis was performed via singular value decomposition (function *propack.svd*, svd package, v0.5.4). Correlations between each principal component (PC) and technical/experimental factors, such as the total number of counts per cell and mouse genotype, were estimated using linear models. Given the strong correlation between the first PC and the total number of counts per cell, we selected PCs 2 to 20 for uniform manifold approximation and projection (UMAP) and clustering analysis. UMAP was generated using the *RunUMAP* function of the Seurat package, while cells were clustered using *FindNeighbors* function followed by *FindClusters*.

Differential expression analysis

Differential expression analysis was conducted using the MAST algorithm (Finak, McDavid et al. 2015) as implemented in the *FindAllMarkers* or *FindMarkers* functions of the Seurat package. *FindAllMarkers*

was employed to identify marker genes specific to each cell cluster while *FindMarkers* was used for other comparative analyses.

CD11b magnetic enrichment for ex vivo analyses

Mice were treated with a single intraperitoneal injection of lipopolysaccharide (LPS) (Sigma, *E.Coli* O55:B5, L6529-1MG) (4 µg/g body weight) or with PBS (saline) as vehicle control for 6 hours for *ex vivo* analyses. Mice were terminally anaesthetized with a combination of Ketamine (100 mg/mL; Nimatek Vet) / Dorbene (medetomidine / hydrochloride; 1 mg/mL; Dorbene vet) and perfused transcardially with PBS. Brains were rapidly dissected and stored in PBS on ice. The olfactory bulb and cerebellum were removed and the brain dissected into small pieces in HBSS (Lonza) in a petri dish. Brain pieces were collected in HBSS, centrifuged and resuspended in an enzymatic mix, following the manufacturer's instructions for the neural dissociation kit (130-092-628, Miltenyi Biotec). After dissociation, cell suspensions were incubated for 20 minutes with CD11b beads (130-049-60, Miltenyi Biotec) and passed through LS columns (130-042-401, Miltenyi Biotec) to enrich microglia by magnetic separation. Lastly, $CD11b^+$ cells were collected and either stained for flow cytometry analyses or treated with RLT lysis buffer for subsequent RNA extraction using the Qiagen RNA isolation kit following the manufacturer's instructions (RNeasy® Mini Kit, 74104, Qiagen).

Human induced pluripotent stem cell-derived microglia

Induced pluripotent stem cells (iPSCs) carrying the c.192G > C mutation in *PARK7* causing the amino acid change p.E64D in DJ-1 and leading to aberrant splicing (Krebiehl, Ruckerbauer et al. 2010, Boussaad, Obermaier et al. 2020) were cultured in mTeSR™ Plus complete medium (Stem Cell Technologies) in 6-well plates. Embryoid bodies (EBs) were generated from iPSCs by supplementing mTeSR™ medium with specific growth factors (**Table S2**). On day 4, EBs were transferred to T75 flasks to form "factories" (van Wilgenburg, Browne et al. 2013). The iPSCs were differentiated into microglia following an established protocol (van Wilgenburg, Browne et al. 2013, Haenseler, Sansom et al. 2017). See **Table S2** for medium composition and growth factors/supplements for each differentiation step. Cells were kept at 37°C in a humidified incubator at 5% CO_2. Microglia-like cells were cultured in 6-well plates at a density of $1x10^6$ cells/well and treated with 100 ng/mL LPS (Sigma, *E.Coli* O55:B5, L6529-1MG) for 6 hours. RNA was extracted using the Qiagen RNA isolation kit following the manufacturer's instructions (RNeasy® Mini Kit, 74104 Qiagen).

Bone marrow-derived macrophage differentiation and treatments

After euthanasia, tibia and femur from *PARK7*/DJ-1 KO mice and wildtype littermates were dissected out and kept in ice-cold DMEM Glutamax (61960526, Gibco) for 1.5-12h before the extraction of bone-marrow cells (BMCs). Both extremities of tibia and femur were cut to allow a 26g needle to flush BMCs according to standardized protocols (Toda, Yamauchi et al. 2021). The cell pellet was treated with NH4Cl (0.17 M) for 5 minutes to remove red blood cells. BMCs were cultured on low-attachment conditions in DMEM

Glutamax (61965026, Gibco), supplemented with 10% FBS (10270-106, Gibco), 1% penicillin-streptavidin (DE17-602E, Lonza), 1 mM sodium pyruvate (11360070, Gibco) and 20 ng/mL M-CSF (416-ML-010/CF, Biotechne). The complete medium was supplemented on day 4. On day 8, fully differentiated bone marrow-derived macrophages (BMDMs) were treated with LPS (100 ng/mL) for 6 hours. To investigate their morphological features, BMDMs were stained with Acti-stain™ 488 Fluorescent Phalloidin (PHDG1, Cytoskeleton, Inc.) and incubated for 1.5 hours at room temperature at day 8 of differentiation with or without prior LPS treatment. Actin cytoskeleton was imaged with a Nikon Eclipse microscope at a 10x magnification and analyzed using CellProfiler™ (Stirling, Swain-Bowden et al. 2021).

RNA sequencing and bioinformatics analyses

Cells were pelleted down and lysed in RLT buffer for subsequent RNA extraction using the Qiagen RNA isolation kit following the manufacturer's instructions (RNeasy® Mini Kit, 74104, Qiagen). A DNase treatment followed by a clean-up has been added using the RNA Clean & Concentrator™-5 kit (Zymo Research) following the manufacturer's instructions. Quantification of total RNA was performed using a N60 Nanophotometer® (Implen GmbH) and a Qubit 2.0 Fluorometer® (Thermo Fisher Scientific) with the Qubit RNA HS Assay Kit. The quality was assessed using a Fragment Analyzer System (Agilent Technologies) using a RNA Pico Chip (Agilent Technologies) (only samples with RQN $\geq$ 7 were further analyzed). The Illumina® stranded Total RNA Prep, Ligation with Ribo-Zero Plus kit Library preparation has been used to process libraries for RNA-sequencing according to Illumina's Reference Guide # 1000000124514 v00 June 2020, starting with 25 ng of total RNA. All libraries have been quantified using a Qubit HS dsDNA kit (Thermo Fisher Scientific) and the library quality check has been performed using a High Sensitivity NGS Fragment Analysis Kit on the Fragment Analyzer System (Agilent Technologies). Indexed libraries were normalized and pooled to be sequenced on an Illumina Novaseq 6000 sequencer according to manufacturer's instructions with targeted conditions of 2 x 75 basepair and 25M reads/sample. For the murine dataset, raw fastq files were quality checked using a combination of *FastQC*, *fastq_screen* and *RSeQC* tools wrapped in *MultiQC v1.11* (Ewels, Magnusson et al. 2016) followed by a preliminary analysis composed of read trimming, mapping and counting using *Cutadapt* (Martin 2011), STAR 2.7.9a (Dobin, Davis et al. 2013) and the Mouse genome (GRCm39 – Mus_musculus.GRCm39.108.gtf). For the human dataset, raw fastq files were quality checked using a combination of *FastQC* and *fastq_screen* tools wrapped in *MultiQC v1.11* (Ewels, Magnusson et al. 2016). Reads were trimmed using *AdapterRemoval v2.3.2* (Schubert, Lindgreen et al. 2016), and mapped against the human genome (Ensembl GRCh38.p14) with the splice-aware STAR 2.7.9a (Dobin, Davis et al. 2013). Resulting alignments were processed by *featureCounts* (package RsubRead v2.8.1) (Liao, Smyth et al. 2019) to obtain gene counts further used by *DESeq2* for differential gene expression. All of these steps were integrated into a local *snakemake* (Molder, Jablonski et al. 2021) environment. The template for the human dataset is available in release 0.3.2: https://gitlab.lcsb.uni.lu/aurelien.ginolhac/snakemake-rna-seq/-/releases/v0.3.2. The software set used by the template on the ULHPC (Varrette et al. 2022) was bundled in a Docker image available at https://hub.docker.com/r/ginolhac/snake-rna-seq tag v0.5. Differential gene expression analysis was conducted using R statistical software v4.2.3 (Team 2021) and DESeq2 v1.38.3 for the murine dataset

and v1.42.0 for the human dataset (Love, Huber et al. 2014) using the resulting gene count tables. Heatmaps were created using *ComplexHeatmap* v2.18.0 (Gu, Eils et al. 2016).

Gene ontology analysis

Differentially expressed genes were submitted to Database for Annotation, Visualization and Integrated Discovery (DAVID) (Sherman, Hao et al. 2022) for further exploration of Gene Ontology (GO) terms for biological processes (BP).

Reverse transcription and qPCR

Reverse transcription was performed using SuperScript™ III (18080093, Invitrogen) according to the manufacturer's instructions. At first, oligo (dT) primers (50 µM) and 5mM dNTP mix were added to the RNA and incubated at 65°C for 5 minutes. Subsequently, tubes were incubated at 4°C for 1 minute and then 5x first-strand buffer, 0.1 M DTT (707265ML, Thermo Fisher Scientific), RNase OUT (10777019, Thermo Fisher Scientific) and 200 units/µl SuperScript™ III RT (18080051, Thermo Fisher Scientific) were added and incubated for 45 minutes at 50°C. The reaction was lastly inactivated by heating for 15 minutes at 70°C. The qPCRs were carried out in 384-well plates (Applied Biosystems QuantStudio5 Real-Time PCR System). All samples were run in three technical triplicates. Diluted cDNA was mixed with 10 µL of Fast SYBR Green Master Mix (Applied Biosystems) and 0.5 µL of 10 µM gene-specific forward and reverse primers. All primers were designed using the Primer BLAST tool with the following parameters: Tm 60°C ± 3°C, possibly spanning exon-exon junctions separated by at least one intron on the corresponding genomic DNA region and a product size between 75-300bp (**Table S3)**. The qPCRs were performed using the following standardized program: 20 seconds at 95°C followed by 35 cycles of PCR stage of 1 second at 95°C (denaturation) and 20 seconds at 60°C (annealing) and a melt curve stage of 15 seconds at 95°C, 1 minute at 60°C and 10 seconds at 95°C. The average threshold cycle (Ct) values were used to quantify the mRNA product by the ΔΔCt method normalized to the housekeeping gene *Gapdh*.

Protein extraction and Western blotting

Protein samples were prepared by lysing whole brain tissues or Magnetic-Activated Cell Sorted (MACS)-$CD11b^+$ cells from wildtype and *PARK7*/DJ-1 KO mice, human fibroblasts and iPSCs in cell lysis buffer (Pierce RIPA, 89900, Thermo Fisher Scientific), supplemented with Halt protease and phosphatase inhibitor (78444, Thermo Fisher Scientific). Protein extracts were then normalized, denatured at 95–100°C for 6–8 minutes, resolved on a 4–12% BisTris gel (NP0323, Lifetech), transferred on polyvinylidene difluoride (PVDF) membranes (LifeTech) and blocked with 2% milk in Tris-buffered saline (TBS) solution containing 0.1% Triton X-100. Anti-DJ-1 (Cell Signaling) was used for protein detection, while anti-α-actin (Merck Millipore) was used for signal normalization. Details of these antibodies can be found in **Table S1**. After washes, the membranes were incubated either with HRP-conjugated secondary antibodies or Rabbit IgG Cross-Adsorbed Secondary Antibody, DyLight™ 800 (SA5-10036, Thermo Fisher Scientific), according to the manufacturer's instructions. Signal development was performed either via addition of Super Signal West Femto Maximum Sensitivity Substrate (Thermo Fisher Scientific) followed by image

acquisition with ImageQuant LAS4010 imaging station (HRP-conjugated secondary antibodies) or via Odyssey Fc Imaging System (LI-COR Biosciences) (Rabbit IgG Cross-Adsorbed Secondary Antibody, DyLight™ 800).

Tissue preparation for immunohistochemistry analyses

Cryosectioning preparation (6-hour LPS time point)

After perfusion with cold PBS, one brain hemisphere per mouse was drop-fixed in 4% paraformaldehyde (PFA, Lonza), washed with PBS and immersed in 30% sucrose (Sigma, SO389) in PBS until complete permeation. When the brain was at the bottom of the tube, it was cut via a rodent brain matrix (ASP Instruments, RBM-2000C) into 4 sagittal macro-sections per hemisphere, which were kept at -80°C until further processing. Subsequently, the macro-sections were embedded in OCT (Tissue-Tek) and cut on a cryostat into 50 µm sections. Tissue sections were mounted on glass slides (Epredia Superfrost™ Plus Adhesion, Epredia™ J1800AMNZ) and washed in PBS.

Floating section preparation (24-hour LPS time point)

After perfusion with cold PBS, the brain was drop-fixed in 4% PFA for 48 hours. Subsequently, brains were stored at 4°C in 0.02% sodium azide/PBS and serialized parasagittal free floating 30 µm-thick sections were generated with a vibratome (Leica; VT-1000S) and collected in cryoprotective medium, PBS containing 1–1 ethylene glycol (Sigma-Aldrich) and 1% w/v polyvinylpyrrolidone (Sigma-Aldrich). Sections were stored at -20°C until further processing.

Immunofluorescence staining

Tissue sections were incubated in 3% H_2O_2 + 1.5% Triton X-100 for 30 minutes and subsequently washed with PBS and blocked in 5% BSA for 30 minutes. Tissue sections were incubated with primary antibodies at room temperature overnight and washed with PBS before incubating them with secondary antibody in 2% BSA 0.3% Triton X-100 for 2 hours at RT (**Table S1**). After washing three times with PBS for 10 minutes, tissue sections were mounted using mounting medium containing 4’,6-diamidino-2-phenylindole (DAPI) (Invitrogen, 00-4959-52) and covered with glass coverslips. Images were acquired using a LSM 880 confocal microscope (Zeiss). iPSCs were plated on coverslips and fixed in 4% PFA for 10 minutes, washed with PBS three times for 5 minutes, subsequently permeabilised and blocked in 3% BSA and 0,4% Triton-X-100 for 1 hour, washed in PBS and incubated overnight with primary antibodies (**Table S1**) in 1% BSA and 0,25% Triton-X-100. Finally, iPSCs were incubated for 2 hours with secondary antibodies and Hoechst and mounted on glass slides.

Image acquisition and application of Microglia and Immune-Cells Morphological Analysis and Clustering (MIC-MAC) 2

Stained slides were imaged on a LSM 880 confocal microscope (Zeiss) with the 20x objective (laser and filters) (the experimenter was blinded for genotype and treatment during acquisition). Nine 3D confocal tile scans were captured with a resolution of 0.221 µm in the x and y dimensions and a resolution of 1 µm in the z dimension. The average thickness per 3D image was 30 µm, and between 28 and 31 µm, depending on the antibody penetration. The resulting 3D stacks of IBA1$^+$ microglial cells were inspected with Imaris and filtered to ensure coherent and high standards of image quality. The 20x 3D images were then processed with Imaris where slice intensities were corrected using the *Normalizer Layer* function, followed by Gaussian Filter (width = 0.3). Segmentation of IBA1$^+$ cells was performed in Imaris by using the *Surface Creation* Tool (*Local Contracts* with *Smooth* enabled and surface detail of 0.5 µm) with a threshold manually adjusted to account for small variations in the contrast of the images (threshold parameter between 0.5 and 1). The *Split Touching Object* option was disabled, and the resulting 3D structures were filtered by size (between 18'000 and 180'000 voxels) to filter out incomplete structures or microglia clusters that would inevitably bias the morphological analysis. For the 24-hour LPS time point, images were captured using a 40x objective with a voxel size of: 0.415 x 0.415 x 0.524 µm^3 with the 405 nm and 633 nm lasers with a pinhole of 42.6 = 1.47 Airy unit (1 µm section). Digital gain DAPI: 1, gain master 860. Offset − 2. A647, Digital gain: 1, Gain master 846 and offset − 7. The morphological feature extraction of each segmented cell was ultimately performed by using *Microglia and Immune-cells Morphological Analysis and Clustering (MIC-MAC) 2*, which allows for automatic segmentation of microglia from 3D fluorescent microscopy images (Fixemer, Ameli et al. 2022).

Statistical analyses

Data was analyzed in Excel and Prism v10.0.3. For qPCR data, fold change from control condition or $2^{-\Delta CT}$ between groups was calculated and compared via 2-way ANOVA with multiple comparisons. Comparison of two groups of normally distributed data was performed using unpaired t-tests. If data did not pass tests for normality using Kolmogorov-Smirnov (alpha = 0.05), a non-parametric Kruskal-Wallis test was performed followed by a multiple comparison test. All experiments included at least 3 biological replicates. All tests were performed on a significance level of 5% and all graphs depict means with standard error of the mean (SEM).

Results

Distinct activation profiles detected by single-cell transcriptional analysis of acutely isolated CD11b $^+$ CD45 ^{int} microglial cells between wildtype and PARK7/DJ-1 KO mice 24 hours after LPS-induced systemic inflammation

First, we confirmed the lack of DJ-1 in the brain of the corresponding KO mice. As expected, while DJ-1 was expressed in the brain tissue of wildtype mice, it was neither detected in brain tissue nor in CD11b$^+$CD45^{int} microglia isolated from *PARK7*/DJ-1 KO mice (**Fig. S1A**). In our previous study, we demonstrated that intraperitoneal injection of LPS at a dosage of 4 µg/g body weight in C57BL/6N mice led to a significant activation of microglial cells after 24 hours (Sousa, Golebiewska et al. 2018). To

investigate the transcriptional profile of microglia under the same inflammatory conditions in mice lacking *PARK7*/DJ-1, we FACS-isolated $CD11b^{+}CD45^{int}$ cells, previously identified as predominantly representing microglia (Sousa, Golebiewska et al. 2018), from both wildtype and *PARK7*/DJ-1 KO mice after 24 hours of LPS injection. Immuno-profiling of the brain under these conditions showed increases in the levels of monocytes ($CD11b^{+}CD45^{+}Ly6C^{+}$ cells) and decreases in the amount of lymphocytes ($CD11b^{-}CD45^{+}$ cells) compared to baseline conditions, indicative of established neuroinflammation at similar levels both in wildtype and *PARK7*/DJ-1 KO mice (**Fig. S1B,C**). We conducted single-cell RNA-sequencing of $CD11b^{+}CD45^{int}$ cells using the Drop-seq technology (Fig. 1A) and performed subsequent clustering analysis of 2'931 microglial cells isolated from *PARK7*/DJ-1 KO and wildtype mice. This approach enabled us to identify five distinct clusters in the corresponding UMAPs (Fig. 1B,C). After identifying differentially expressed genes (DEGs) that characterize each cluster compared to the others, we conducted gene ontology (GO) term enrichment analysis by submitting the up-regulated DEGs from each cluster (adjusted p-value < 0.05, log2FC ≥ 0.5) to DAVID (**Table S4**). The resulting GO term for Cluster 1 included "synapse disassembly", while Cluster 2 was characterized by terms related to transcriptional regulation, such as "RNA splicing", "chromatin organization" and "mRNA processing" (**Fig. S1D**). Cluster 3 was defined by GO terms related to classical inflammatory responses, including "cellular response to interleukin-1" and "lipopolysaccharide-mediated signalling pathway", with upregulation of microglial pro-inflammatory markers (e.g. *Gpr84*, *Lcn2* and *Nfkbia*) (Fig. 1D), while Cluster 4 was characterized by terms linked to DNA damage response, such as "DNA replication" and "DNA repair", with overexpression of homeostatic microglial genes (e.g. *Hexb*, *Fcrls* and *Gpr34*) and DNA repair markers (e.g. *Brca2*, *Parp1* and *Rrm1*) (Fig. 1E). Lastly, Cluster 5 was associated with GO terms related to host defense responses, primarily against viruses, including "defense response to virus" and "cellular response to interferon-beta" (**Fig. S1D**) (**Table S4**). We showed a selection of DEGs (considering adjusted p-value < 0.05, |log2FC| > 0.5) characterizing each cluster in a dot plot (Fig. 1F). When examining the composition of each cluster based on the amount of cells per mouse genotype using an alluvial plot (Fig. 1G) and analyzing the corresponding ratios using a heatmap (Fig. 1H), we observed that clusters 1, 2 and 5 were relatively equally represented in both genotypes. In contrast, Cluster 3, associated with classical inflammatory responses, was predominantly constituted by microglial cells from wildtype mice (85%), whereas Cluster 4, linked to DNA damage response, primarily consisted of cells originating from *PARK7*/DJ-1 KO mice (81%) (Fig. 1G,H).

Taken together, these results show that microglia in wildtype mice display a classical inflammatory profile following 24 hours of LPS injection, characterized by substates associated to transcriptional regulation (Cluster 2) and pro-inflammatory responses (Cluster 3), while microglia in *PARK7*/DJ-1 KO mice show an enrichment in DNA damage response signatures (Cluster 4), suggesting a potential involvement in repair and tolerance mechanisms.

Diverse transcriptional activation profiles of microglia detectable after 6 hours of peripheral LPS-induced inflammation in PARK7/DJ-1 KO compared to wildtype mice

Next, we sought to investigate whether the distinct microglial profiles identified after 24 hours of LPS-induced inflammation were also apparent at earlier time points. With this analysis, we aimed to discern if the impaired microglial reactivity under *PARK7*/DJ-1 deficiency manifested during the early phases of the inflammatory response or if they indicated premature resolution substates. For this, we intraperitoneally injected *PARK7*/DJ-1 KO and wildtype mice with LPS (4 µg/g body weight) and MACS-isolated $CD11b^+$ cells from dissected brains after 6 hours for subsequent transcriptional analyses (**Fig. S2A**). We verified the validity of our sorting protocol by analyzing the expression levels of oligodendrocyte (*Mog* and *Mobp*), astrocyte (*Gfap* and *Ntsr2*) and neuronal (*Tubb3* and *NeuN*) markers in MACS-isolated $CD11b^+$ cells compared to the negative fraction. Those markers were undetectable or only expressed at very low levels in cells collected within the positive fraction, which on the contrary expressed high levels of the microglial markers (*Gpr34* and *Olfml3*) (**Fig. S2B**). We tested the purity of $CD11b^+$ cells by staining plated sorted cells with IBA1 antibody and detected 90–97% (mean 94.5% ± 1.9%) of $IBA1^+$ cells among $CD11b^+$ cells, thus indicating an enrichment of microglial cells (**Fig. S2C**). By conducting RNA-sequencing analyses of MACS-isolated $CD11b^+$ cells from *PARK7*/DJ-1 KO and age-matched wildtype mice following 6 hours of LPS injection, we detected DEGs (p-value < 0.05, $|\log2FC| \geq 0.5$) comparing KO versus wildtype. Among them, 227 genes were upregulated, while 247 genes were downregulated (**Table S5)**. GO terms resulting from the 227 upregulated DEGs comparing $CD11b^+$ cells isolated from *PARK7*/DJ-1 KO and wildtype mice in response to LPS were “membrane depolarization”, “signal transduction” and “apoptotic signaling pathway” (Fig. 2A). On the other hand, GO terms resulting from the corresponding 247 downregulated DEGs were linked to the immune response, mainly related to the regulation of the adaptive immune system, such as “adaptive immune response” and “negative regulation of T cell proliferation”, and interferon-gamma-related pathways, exemplified by “interferon-gamma production” and “cellular response to interferon-gamma” terms (Fig. 2B). Among the related down-regulated genes, *Tnfrsf9, Ciita, Serpina3g, Ifng* and *H2.Aa* were in the top 50 protein-coding DEGs (Fig. 2C).

The characterization of these distinct profiles under LPS treatment prompt us to investigate whether differences between microglial cells in *PARK7*/DJ-1 KO and wildtype mice were already detectable at baseline. Through RNA-sequencing analysis of MACS-isolated $CD11b^+$ cells from *PARK7*/DJ-1 KO and age-matched wildtype mice, we detected 308 DEGs (p-value < 0.05, $|\log2FC| \geq 0.5$) comparing KO versus wildtype. Among them, 103 genes were upregulated, while 205 genes were downregulated (**Table S5**). GO terms resulting from the 103 upregulated DEGs comparing $CD11b^+$ cells isolated from *PARK7*/DJ-1 KO and wildtype mice at baseline were mainly related to developmental processes and morphological adaptation, such as “epithelial cell differentiation”, “extracellular matrix organization” and “branching morphogenesis of an epithelial tube” (Fig. 2D), while terms resulting from the corresponding 205 downregulated DEGs included differentiation and immune response (Fig. 2E). Among the related down-regulated genes, *Cxcl9* and *Ifi214*, linked to the interferon-gamma signaling, were in the top 50 protein-coding DEGs (Fig. 2F). We confirmed the decrease of the expression levels of these genes by qPCR using independent $CD11b^+$ brain cell-derived RNA samples (**Fig. S2C**).

Taken together, these results show that microglia in *PARK7*/DJ-1 KO mice downregulate genes associated with inflammatory responses, specially linked to interferon-gamma signaling, both at the early stages of inflammatory conditions and at baseline, compared to wildtype mice. On the other hand, microglia in *PARK7*/DJ-1 KO mice treated for 6 hours with LPS upregulate genes related to “membrane depolarization”, “signal transduction” and “apoptotic signalling pathway”, which, in line with the described functions of DJ-1 as an important protector against ROS and the DNA damage response signatures identified after 24 hours of LPS treatment by scRNA-sequencing (Cluster 4), are related to repair and tolerance mechanisms, such as attenuation of mitochondrial reactive oxygen species generation (Sack 2006).

Discrete activated transcriptional profile of microglia derived from iPSCs harboring the c.192G > C mutation in PARK7 compared to isogenic controls 6 hours after LPS treatment

Next, to investigate whether these findings hold true in the human context, we applied a translational approach to verify if the microglial transcriptional phenotype identified in *PARK7*/DJ-1 KO mice was similar in human *PARK7*/DJ-1 mutant iPSC-derived microglia. Briefly, iPSCs carrying the c.192G > C mutation in *PARK7* causing the amino acid change p.E64D in DJ-1 were previously described to lead to undetectable levels of DJ-1 protein in these cells due to aberrant splicing (Boussaad, Obermaier et al. 2020). Both isogenic control and mutant iPSCs expressed similar levels of the typical pluripotency markers, including stage-specific embryonic antigen-4 (SSEA4), podocalyxin (TRA-1-60), octamer-binding transcription factor 4 (OCT4) and sex determining region-Y box (SOX2), thus suggesting that *PARK7*/DJ-1 deficiency does not affect their expression (**Fig. S3A,B**). As expected, while we measured high levels of *PARK7*/DJ-1 expression in isogenic control fibroblasts and iPSCs, both at the protein and mRNA level, its expression was not detectable in the corresponding mutant cells (**Fig. S3C,D**). We derived microglial cells from iPSCs following an established protocol (van Wilgenburg, Browne et al. 2013, Haenseler, Sansom et al. 2017). Analysis of *PARK7* in the resultant iPSC-derived microglia (iMG) confirmed the lack of its expression in the mutant cells (**Fig. S3C**). Gene expression analyses of three human microglia homeostatic genes, *GPR34*, *TREM2* and *P2RY12*, in both isogenic control and mutant cultures, showed increased expression levels in iMG when compared to undifferentiated iPSCs, thus indicating effective differentiation of the two lines into microglia-like cells (**Fig. S3E**).

As conducted in the mouse model, we carried out RNA sequencing to compare the transcriptional signatures of *PARK7*/DJ-1 mutant and isogenic control iMG, both with or without a LPS (100 ng/mL) treatment for 6 hours, which resulted in relatively distinct clusters according to the four conditions (Fig. 3A). At baseline, among 197 DEGs (adjusted p-value < 0.05, $|\log2FC| \geq 0.5$) (**Table S6**), we detected 103 upregulated genes in *PARK7*/DJ-1 mutant iMG. GO terms associated to those upregulated genes included “cell adhesion”, “proteolysis” and “extracellular matrix organization” (Fig. 3B). By contrast, GO analysis of the 94 downregulated genes comprised terms linked to immune responses, such as “cellular response to lipopolysaccharide” and “positive regulation of interferon-gamma production” (Fig. 3C), thus indicating an effect on microglial immune surveillance and activation already at baseline. We showed a selection of corresponding up- (e.g., *CPA4, PCDHGB5, LOXL4*) and down- (e.g., *NLRP2, S100A6, ACOD1, IFI44*)

regulated genes (adjusted p-value < 0.05, |log2FC| ≥ 0.5) characterizing *PARK7*/DJ-1 mutant iMG in a dot plot (Fig. 3D).

Under LPS conditions, we detected 289 DEGs (adjusted p-value < 0.05, |log2FC| ≥ 0.5), when comparing *PARK7*/DJ-1 mutant and isogenic control iMG (**Table S6**). Among them, 83 genes were upregulated, while 206 were downregulated in *PARK7*/DJ-1 mutant iMG. GO analyses of up-regulated genes showed terms associated with long-chain fatty acid metabolism and cell adhesion (Fig. 3E), while corresponding analyses of down-regulated genes resulted in terms related to immune responses, including “defense response to virus”, “cellular response to lipopolysaccharide” and “positive regulation of interferon-beta production” (Fig. 3F). We displayed a selection of resulting up- (e.g., *CLMP, PCDHGB5, HTRA1, ADAM8*) and down-regulated (e.g., *S100A6, NLRP2, ACOD1*) genes (adjusted p-value < 0.05, |log2FC| ≥ 0.5) characterizing *PARK7*/DJ-1 mutant iMG treated with LPS using a dot plot (Fig. 3G). Interestingly, some of these genes were commonly up- (e.g., *CLMP, HTRA1, ADAM8*) or down-regulated (e.g., *ACOD1, S100A6, NLRP2*) both at baseline and LPS conditions comparing *PARK7*/DJ-1 mutant and isogenic control iMG (**Fig. S3F**).

Overall, these results show that *PARK7*/DJ-1 mutant iMG, in line with the analogous murine cells, display an attenuated response to LPS compared to corresponding isogenic control cells.

Enhanced compactness at baseline and less pronounced amoeboid morphology of microglia in PARK7/DJ-1 KO compared to wildtype mice after 6 and 24 hours of LPS treatment

Since the identified distinct microglial gene expression patterns may represent morphological phenotypes evident in brain tissues, we investigated microglial morphological changes in *PARK7*/DJ-1 KO and wildtype mice at baseline and under LPS conditions. To this end, we stained brain tissues with an antibody against the microglial marker ionized calcium-binding adapter molecule 1 (IBA1) and applied MIC-MAC 2 to the resulting 3D confocal images in order to segment and classify microglial cells based on their morphology (Salamanca, Mechawar et al. 2019, Fixemer, Ameli et al. 2022). While, homeostatic surveying microglia were highly ramified with multiple processes (nodes), activated microglia show a more amoeboid and compact shape. Using MIC-MAC 2, we were able to extract morphological features based on the shape, structure and size of microglia, enabling to score the cells based on the levels of their roundness or elongation.

Within the analyzed cortical regions, we recognized five distinct morphological clusters that were differentially represented in *PARK7*/DJ-1 KO and wildtype mice at baseline and after 6 hours of LPS-treatment (Fig. 4A). Corresponding quantifications showed decreased ratios of ramified microglia (Cluster 1) and enhanced proportions of amoeboid microglia (Cluster 5) in *PARK7*/DJ-1 KO compared with wildtype mice at baseline (Fig. 4B). Under LPS conditions, the ratio of amoeboid microglia (Cluster 5) was increased compared to baseline conditions, although this rise was less prominent in *PARK7*/DJ-1 KO compared with wildtype mice (Fig. 4B). We further confirmed these results by coupling the analysis of relevant features, including compactness and node density, across the various conditions. Indeed, cortical microglia were more amoeboid and less ramified (fewer nodes) at baseline, while they were less

amoeboid and more ramified after 6 hours LPS-treatment in *PARK7*/DJ-1 KO compared with wildtype mice (Fig. 4C). In line with these observations, the intensity of IBA1 expression per area was higher in wildtype compared with *PARK7*/DJ-1 KO brains 6 hours after LPS treatment, indicating a higher activation rate of microglia in wildtype mice (Fig. 4D). By similarly investigating morphological changes of microglia 24 hours following LPS treatment, we detected higher compactness and lower node density of cortical microglia in wildtype compared to *PARK7*/DJ-1 KO mice (Fig. 4E,F). This trend was even more evident in the *substantia nigra*, a brain region that is primarily affected in PD (Fig. 4G), indicating a more prominent effect of *PARK7*/DJ-1 KO deficiency in microglial morphological adaptation in PD-related brain regions.

Taken together, our results show that microglia in *PARK7*/DJ-1 deficient mice display different morphologies at baseline and exhibit a distinct morphological adaptation in response to inflammation characterized by a reduced reaction towards LPS-induced inflammation compared to wildtype microglia after 6 and 24 hours of systemic LPS treatment.

Type II interferon-related gene impairment, prominent compactness at baseline and less evident amoeboid morphology after LPS treatment detectable in bone marrow-derived macrophages comparing precursor cells isolated from PARK7/DJ-1 KO and wildtype mice

Lastly, to study if the identified murine *ex vivo* and human *in vitro* microglial transcriptional profiles under *PARK7*/DJ-1 KO deficiency are specific to brain cells or are also detectable in peripheral myeloid cells, we isolated bone marrow cells from the femurs and tibia of *PARK7*/DJ-1 KO and wildtype mice and differentiated them for 7 days into macrophages (Toda, Yamauchi et al. 2021). First, we verified that cells lacking *PARK7*/DJ-1 were effectively differentiated into macrophages by analyzing the expression levels of CD11b and F4/80, which indeed did not differ from wildtype cells and represented 95–98% of total cells (Fig. 5A). Further, the expression levels of *Adgre1*, coding for F4/80, did not show differences between the two genotypes (Fig. 5B). As detected in microglia at baseline, bone marrow-derived macrophages (BMDMs) from *PARK7*/DJ-1 KO mice showed decreased expression levels of *Cxcl9* and *Ifi214* compared to corresponding cells isolated from wildtype mice (Fig. 5C). Following exposure of BMDMs to LPS (100 ng/mL) for 6 hours, cells from *PARK7*/DJ-1 KO mice, as previously demonstrated in microglia, showed decreased expression levels of *Ciita* compared to cells from wildtype mice (Fig. 5D). Notably, in line with the observations we made in mouse brain slices, we detected prominent morphological differences between macrophages originating from *PARK7*/DJ-1 KO and wildtype mice, with KO macrophages showing enhanced compactness at baseline and a less evident amoeboid shape following 6 hours of LPS exposure compared to wildtype cells (Fig. 5E).

Overall, these results are in agreement with the previously characterized microglial transcriptional signatures and morphological adaptations detected in the mouse brain, showing that BMDMs under *PARK7*/DJ-1 deficiency display a reduced IFNrelated signature, both at baseline and after LPS exposure, as well as display similar morphological alterations.

Discussion

At first PD diagnosis, it has been estimated that 30–50% of dopaminergic neurons in the *substantia nigra* have already degenerated (Cheng, Ulane et al. 2010, Burke and O'Malley 2013). Therefore, for diagnostic and therapeutic perspectives, it is crucial to explore occurrences in prodromal PD phases, the period preceding a PD diagnosis, during which neuroinflammatory processes are already taking place (Tansey, Wallings et al. 2022, Terkelsen, Klaestrup et al. 2022). Thus, in the present study we address this challenge by investigating transcriptional and morphological changes of microglia in a prodromal model of PD, the *PARK7*/DJ-1 KO mouse, at 3–4 months, an age corresponding to adulthood in humans (Dutta and Sengupta 2016), where motor symptoms are not manifested yet (Pham, Giesert et al. 2010).

The large majority of studies investigating the functions of DJ-1 in microglia were so far conducted in immortalized microglial cell lines showing that *PARK7*/DJ-1 deficiency sensitizes cells resulting in an exaggerated response to LPS *in vitro* (Trudler, Weinreb et al. 2014, Lind-Holm Mogensen, Scafidi et al. 2023). In our study, we conducted *in vivo* and *ex vivo* analyses, thus achieving a more comprehensive view of the brain, corroborating our findings using translational *in vitro* models. We previously showed that the downregulation of homeostatic markers and upregulation of classical inflammatory genes represent a typical transcriptional signature of microglia in a LPS model of neuroinflammation (Sousa, Golebiewska et al. 2018). Here, we show that microglia in *PARK7*/DJ-1 KO mice display a distinct response to LPS, specifically characterized by an attenuated inflammatory transcriptional program, which is also recapitulated in human *PARK7*/DJ-1 mutant iPSC-derived microglia (iMG). Among the impaired pathways, we detected a downregulation of genes related to interferon signaling, at baseline and following LPS treatment in both models. Specifically, in microglia isolated from *PARK7*/DJ-1 KO mice, we detected a downregulation of interferon-related genes, both at steady state (e.g. *Cxcl9, Tnfrsf9* and *Ifi214*) and after 6 hours (e.g. *Ciita, Ifng, H2-Aa, Oasl2, Gbp8, Ifi213, Ifi27l2a, Tgtp2*) or 24 hours (e.g. *Ifitm3, Irf7*) following LPS treatment, aligning with patterns also observed in long-term/chronic stress models (Sonnenfeld, Cunnick et al. 1992, Zhang, Dong et al. 2022). In the DJ-1 mutant iMG, *S100A6, NLRP2* and *ACOD1* were among the most downregulated genes, both at baseline and after LPS treatment. Interestingly, *S100A6* is a gene known to be involved in cellular stress responses and regulation of cytoskeletal functions (Wang, Kang et al. 2023). *ACOD1* is a key gene involved in immunometabolism coding for an enzyme converting the TCA cycle intermediate cis-aconitate into itaconate, which possesses anti-microbial properties (Michelucci, Cordes et al. 2013). Of note, *ACOD1* expression is induced by interferon regulating factor 1 (IRF1) (Tallam, Perumal et al. 2016), thus its decrease can be linked to the impairment of the interferon signaling pathway. Furthermore, *ACOD1* is also an important mediator of mitochondrial ROS generation (Hall, Boyle et al. 2013), hence the downregulation of this gene could be a way of adjusting for the loss of DJ-1 in microglia. Previous studies reported excessive inflammatory reaction of DJ-1 deficient astrocytes and microglia to IFN-γ (Kim, Choi et al. 2013) and LPS (Waak, Weber et al. 2009, Meiser, Delcambre et al. 2016, Lin, Chen et al. 2021). Briefly, DJ-1 can bind src-homology 2-domain containing protein phosphatase (SHP-1) and inhibit signal transducer and activator of transcription 1 (STAT-1) signaling in microglia and astrocytes, dampening the inflammatory response initiated via STAT-1 (Kim, Choi et al. 2013). The downregulation of IFN-related genes at baseline and after

LPS-treatment in microglia from *PARK7*/DJ-1 KO mice may represent a compensatory mechanism aimed at avoiding an excessive neurotoxic response via the activation of STAT-1 and NFκB. Along these lines, higher levels of glutathione (GSH) have been detected in the medial prefrontal cortex of *PARK7*/DJ-1 KO compared to wildtype mice, which might signify a compensatory mechanism to overcome the loss of the anti-oxidative properties of DJ-1 (Chen, Liu et al. 2022). Interestingly, changes in GSH metabolism have been observed in various PD patients (Bjorklund, Peana et al. 2021). This is possibly happening in astrocytes, as those glial cells are known to be important for feeding neurons with precursors for GSH synthesis (Perez-Sala and Pajares 2023). In our study, we did not detect upregulation of genes related to the anti-oxidative machinery, neither in murine nor in iMG. However, as we aimed to focus on the effect of the loss of *PARK7*/DJ-1 in microglia, we cannot exclude that compensatory mechanisms took place in surrounding CNS cells. We, therefore, hypothesize that the downregulation of IFN-related genes and upregulation of DNA repair markers, which can be related to tolerogenic mechanisms (Giglia-Mari, Zotter et al. 2011), keep the loss of DJ-1 and oxidative stress in check. However, at a certain stage, representing a “tipping point”, the CNS environment and microglial cells are no longer able to compensate for the loss of *PARK7*/DJ-1 leading to neuroinflammation and neurodegeneration as a consequence of inflammageing and chronic disturbance of the redox balance.

In addition to the attenuated inflammatory response at the transcriptional level, we found discrete morphological adaptations comparing the classical amoeboid shape of microglia after LPS treatment. The understanding of microglial physiology in relation to its morphology is generally limited and the shape of microglia only partly reflect their functions (Bosch and Kierdorf 2022). However, there is consensus on the overarching patterns and correlations between the shape of microglia and certain conditions, such as a less ramified and more compact amoeboid shape is considered an activated microglia reacting to danger or damage signals, whereas a highly ramified structure is considered a feature of surveying homeostatic microglia (Vidal-Itriago, Radford et al. 2022). Our study found changes in gene ontologies related to cytoskeleton and extracellular matrix reorganization, both in *PARK7*/DJ-1 KO mice and human iPSC-derived DJ-1 mutant microglia. A previous study deeply investigated and described reduced microtubules in DJ-1 deficient neurons (Sheng, Heng et al. 2013). More specifically, *PARK7*/DJ-1 deficient mice exhibited a decreased dendritic complexity with reduced dendritic spine densities in medium spiny neurons (Sheng, Heng et al. 2013). This was found to be a consequence of the downregulation of β-tubulin-III, an important regulator of microtubules, which is regulated by HIF1α. In our study, we found a decreased complexity of microglial processes under steady state conditions in the cortex and *substantia nigra* of *PARK7*/DJ-1 KO mice, which had a more compact shape with thicker and less processes as well as a larger soma. This hyper ramified morphology was previously observed in microglia in various chronic stress models, where stress was shown to increase microglial internal complexity and degree of branching (Hinwood, Tynan et al. 2013, Smith, Kassem et al. 2019). Importantly, these observations are in line with the detected impaired interferon-related signatures related to stress conditions at the transcriptional level. As microglial coverage and processes are essential for immunosurveillance, we hypothesize that the reduced complexity of microglia observed in *PARK7*/DJ-1 KO mice at baseline might affect their functions, including altering their communication with other CNS

cells and their surveillant features of the brain parenchyma. The pivotal factors influencing process extensions and cell migration involve adhesive interactions with the surrounding extracellular matrix. In this perspective, we found an upregulation of genes related to proteolysis, cell adhesion and extracellular matrix organization both in microglia from *PARK7*/DJ-1 KO mice (e.g. *Adamts13, Elf3*) and in human DJ-1 mutant iMG (e.g. *CPA4, ADAM8, CAPN3, HTRA1, CLMP, COL6A3, COL4A1*). These findings suggest that microglia under *PARK7*/DJ-1 deficiency might be more active in the degradation of the extracellular matrix and the secretion of proteins involved in adhering and interacting with the matrix compared to their normal counterparts.

The distinct microglial phenotypic acquisition under *PARK7*/DJ-1 deficiency, both at baseline and following a LPS treatment, might play a role in fostering dopaminergic cell death and amplifying the damage to those vulnerable neurons over time. In fact, a precise balance between an efficient and timely response to infections without compromising the fine-tuned neuronal network is essential for a healthy CNS. Following the impairment of IFN-related pathways that we detected both in the mouse and human models, it would be interesting to further investigate the role of DJ-1 in additional infectious paradigms, such as in viral models. A dampened CNS immune response towards microbial threats under *PARK7*/DJ-1 deficiency could render prodromal PD individuals more susceptible to CNS or systemic infections, thus impacting the brain.

Conclusions

In summary, our investigations provide a comprehensive transcriptional and morphological analysis of microglia in *PARK7*/DJ-1 KO mice under steady state and inflammatory conditions that we also complement for translational prospects in human *PARK7*/DJ-1 mutant iMG. Our results suggest that microglial cells under *PARK7*/DJ-1 deficiency react differently to an inflammatory stimulus, specifically dampening the interferon-related pathway at the transcriptional level and regulating actin dynamics and cell cytoskeleton affecting their classical amoeboid activated phenotypic state. Furthermore, we detected an impairment of the interferon response at baseline, which is associated with a hyper ramified morphology representing typical features of microglia under chronic stressful conditions. Taken together, our findings suggest that the underlying chronic oxidative stress associated to the lack of *PARK7*/DJ-1 at baseline affects microglia neuroinflammatory responses, which may play a causative role in PD onset and progression. Further studies are warranted to investigate how the identified molecular and morphological cues underlying *PARK7*/DJ-1 deficiency affect key microglial functions, including their phagocytic activity and communication with the underlying neuronal network.

Abbreviations

BMC: Bone marrow cell

BMDM: Bone marrow-derived macrophage

BP: Biological Processes

CNS: Central nervous system

DAPI: 4',6-diamidino-2-phenylindole

DAVID: Database for Annotation, Visualization and Integrated Discovery

DEGs: Differentially expressed genes

DJ-1: Protein deglycase-1, Parkinsonism associated deglycase-1 (*PARK7*)

EB: Embryoid bodies

FACS: Fluorescence-Activated Cell Sorting

Gfap: glial fibrillary acidic protein

GO: Gene ontology

Gpr34: G-protein coupled receptor 34

GSH: glutathione

HBSS: Hanks' Balanced Salt Solution

IBA1: Ionized calcium-binding adapter molecule 1 (also known as allograft inflammatory factor 1)

IFN-γ: Interferon gamma

iMG: Induced pluripotent stem cell-derived microglia-like cell

iPSC: Induced pluripotent stem cell

IRF1: Interferon regulating factor 1

KO: Knockout

LPS: Lipopolysaccharide

MACS: Magnetic-Activated Cell Sorting

MIC-MAC: Microglia and Immune Cell Morphologies Analyser and Classifier

Mog: myelin oligodendrocytic glycoprotein

Mobp: myelin associated oligodendrocyte basic protein

NeuN: Neuronal nuclei

Ntsr2: Neurotensin receptor 2

OCT4: Octamer-binding transcription factor 4

Olfml3: Olfactomedin like 3

UMAP: Uniform Manifold Approximation and Projection

Park7: *Parkinsonism associated deglycase 7*

PBS: Phosphate Buffered Saline

PCA: Principal Component Analysis

PD: Parkinson's disease

RT-qPCR: Reverse Transcription Quantitative Polymerase Chain Reaction

SEM: Standard error of the mean

SHP-1: Src-homology 2-domain containing protein phosphatase

SOX2: Sex determining region-Y box

SSEA4: Stage-specific embryonic antigen-4

STAT-1: Signal transducer and activator of transcription 1

TGFβ: Tumor growth factor-β

TNF: Tumor necrosis factor

TRA-1-60: Podocalyxin

Tubb3: Tubulin 3

Declarations

Ethical approval and consent to participate

All animal experiments were performed according to all applicable laws and regulations (EU Directive 2010/63/EU and Grand-Ducal Regulation of 11 January 2013 on the protection of animals used for scientific purposes), after receiving approval for the animal license (reference number: LUPA2022/1) from the Animal Experimentation Ethics Committee at the University of Luxembourg (AEEC) and the Ministry of

Agriculture, Viniculture and Rural Development. Experiments on iPSCs were conducted in accordance with the ethics rules at the University of Luxembourg.

Consent for publication

Not applicable.

Acknowledgements

We are grateful to Ms. Amandine Bernard for mouse genotyping and technical support with Western blotting as well as to Ms. Virginie Baus for helping with the cryostat tissue cutting. We would also like to thank Dr Eduardo Rosales Jubal for advices on statistical analyses of qPCR and MIC-MAC results.

Funding

FL-HM was supported by the Luxembourg National Research Fund (FNR) through the FNR-PRIDE program i2TRON for doctoral education (PRIDE/14254520/I2TRON). C.S. was supported by the FNR (AFR/6916713) and the Fondation du Pélican de Mie et Pierre Hippert-Faber under the aegis of Fondation de Luxembourg. C.A. was supported by the FNR-PRIDE program CriTiCS for doctoral education (PRIDE/10907093/CRITICS) and the CMCM (Caisse Médico-Complémentaire Mutualiste Luxembourg) matching grant. W.W. was supported by the Deutsche Zentrum für Psychische Gesundheit (DZPG), site Munich-Augsburg. A.S. was supported by the FNR through the INTER/DFG/17/11583046 grant. For the purpose of open access, and in fulfilment of the obligations arising from the FNR grant agreement, the author has applied a Creative Commons Attribution 4.0 International (CC BY 4.0) license to any Author Accepted Manuscript version arising from this submission.

Author's Contributions

Conceptualization, FL-HM, and AlM; Methodology, FL-HM, CS, CA, KB, ArM, TK, DC, AnS, SKP, NC, AuG, DMVW, WW, AP, PVN, AlS, AnG, and AlM; Formal analysis, FL-HM, CS, CA, TK, ArM, KB, AuG; Supervision: PVN, AlS, AnG, and AlM; Writing – original draft preparation, FL-HM, and AlM; Writing – review, and editing, all authors; Data curation, FL-HM, and AlM; Funding acquisition, AlM. All authors read and approved the final version of the manuscript.

Competing interests

The authors declare no competing interests.

References

1. Bjorklund, G., M. Peana, M. Maes, M. Dadar and B. Severin (2021). "The glutathione system in Parkinson's disease and its progression." Neurosci Biobehav Rev **120**: 470-478.

2. Bosch, L. F. P. and K. Kierdorf (2022). "The Shape of mu-How Morphological Analyses Shape the Study of Microglia." Front Cell Neurosci **16**: 942462.
3. Boussaad, I., C. D. Obermaier, Z. Hanss, D. R. Bobbili, S. Bolognin, E. Glaab, K. Wolynska, N. Weisschuh, L. De Conti, C. May, F. Giesert, D. Grossmann, A. Lambert, S. Kirchen, M. Biryukov, L. F. Burbulla, F. Massart, J. Bohler, G. Cruciani, B. Schmid, A. Kurz-Drexler, P. May, S. Duga, C. Klein, J. C. Schwamborn, K. Marcus, D. Woitalla, D. M. Vogt Weisenhorn, W. Wurst, M. Baralle, D. Krainc, T. Gasser, B. Wissinger and R. Kruger (2020). "A patient-based model of RNA mis-splicing uncovers treatment targets in Parkinson's disease." Sci Transl Med **12**(560).
4. Bu, X. L., X. Wang, Y. Xiang, L. L. Shen, Q. H. Wang, Y. H. Liu, S. S. Jiao, Y. R. Wang, H. Y. Cao, X. Yi, C. H. Liu, B. Deng, X. Q. Yao, Z. Q. Xu, H. D. Zhou and Y. J. Wang (2015). "The association between infectious burden and Parkinson's disease: A case-control study." Parkinsonism Relat Disord **21**(8): 877-881.
5. Burke, R. E. and K. O'Malley (2013). "Axon degeneration in Parkinson's disease." Exp Neurol **246**: 72-83.
6. Chen, L., B. Cagniard, T. Mathews, S. Jones, H. C. Koh, Y. Ding, P. M. Carvey, Z. Ling, U. J. Kang and X. Zhuang (2005). "Age-dependent motor deficits and dopaminergic dysfunction in DJ-1 null mice." J Biol Chem **280**(22): 21418-21426.
7. Chen, W., H. Liu, S. Liu, Y. Kang, Z. Nie and H. Lei (2022). "Altered prefrontal neurochemistry in the DJ-1 knockout mouse model of Parkinson's disease: complementary semi-quantitative analyses with in vivo magnetic resonance spectroscopy and MALDI-MSI." Anal Bioanal Chem **414**(28): 7977-7987.
8. Cheng, H. C., C. M. Ulane and R. E. Burke (2010). "Clinical progression in Parkinson disease and the neurobiology of axons." Ann Neurol **67**(6): 715-725.
9. Clements, C. M., R. S. McNally, B. J. Conti, T. W. Mak and J. P. Ting (2006). "DJ-1, a cancer- and Parkinson's disease-associated protein, stabilizes the antioxidant transcriptional master regulator Nrf2." Proc Natl Acad Sci U S A **103**(41): 15091-15096.
10. Dobin, A., C. A. Davis, F. Schlesinger, J. Drenkow, C. Zaleski, S. Jha, P. Batut, M. Chaisson and T. R. Gingeras (2013). "STAR: ultrafast universal RNA-seq aligner." Bioinformatics **29**(1): 15-21.
11. Dorsey, E. R., T. Sherer, M. S. Okun and B. R. Bloem (2018). "The Emerging Evidence of the Parkinson Pandemic." J Parkinsons Dis **8**(s1): S3-S8.
12. Dutta, S. and P. Sengupta (2016). "Men and mice: Relating their ages." Life Sci **152**: 244-248.
13. Ewels, P., M. Magnusson, S. Lundin and M. Kaller (2016). "MultiQC: summarize analysis results for multiple tools and samples in a single report." Bioinformatics **32**(19): 3047-3048.
14. Fang, F., K. Wirdefeldt, A. Jacks, F. Kamel, W. Ye and H. Chen (2012). "CNS infections, sepsis and risk of Parkinson's disease." Int J Epidemiol **41**(4): 1042-1049.
15. Finak, G., A. McDavid, M. Yajima, J. Deng, V. Gersuk, A. K. Shalek, C. K. Slichter, H. W. Miller, M. J. McElrath, M. Prlic, P. S. Linsley and R. Gottardo (2015). "MAST: a flexible statistical framework for assessing transcriptional changes and characterizing heterogeneity in single-cell RNA sequencing data." Genome Biol **16**: 278.

16. Fixemer, S., C. Ameli, G. Hammer, L. Salamanca, O. Uriarte Huarte, C. Schwartz, J. J. Gerardy, N. Mechawar, A. Skupin, M. Mittelbronn and D. S. Bouvier (2022). "Microglia phenotypes are associated with subregional patterns of concomitant tau, amyloid-beta and alpha-synuclein pathologies in the hippocampus of patients with Alzheimer's disease and dementia with Lewy bodies." Acta Neuropathol Commun **10**(1): 36.
17. Gerhard, A., N. Pavese, G. Hotton, F. Turkheimer, M. Es, A. Hammers, K. Eggert, W. Oertel, R. B. Banati and D. J. Brooks (2006). "In vivo imaging of microglial activation with [11C](R)-PK11195 PET in idiopathic Parkinson's disease." Neurobiol Dis **21**(2): 404-412.
18. Giglia-Mari, G., A. Zotter and W. Vermeulen (2011). "DNA damage response." Cold Spring Harb Perspect Biol **3**(1): a000745.
19. Goldberg, M. S., A. Pisani, M. Haburcak, T. A. Vortherms, T. Kitada, C. Costa, Y. Tong, G. Martella, A. Tscherter, A. Martins, G. Bernardi, B. L. Roth, E. N. Pothos, P. Calabresi and J. Shen (2005). "Nigrostriatal dopaminergic deficits and hypokinesia caused by inactivation of the familial Parkinsonism-linked gene DJ-1." Neuron **45**(4): 489-496.
20. Gu, Z., R. Eils and M. Schlesner (2016). "Complex heatmaps reveal patterns and correlations in multidimensional genomic data." Bioinformatics **32**(18): 2847-2849.
21. Haenseler, W., S. N. Sansom, J. Buchrieser, S. E. Newey, C. S. Moore, F. J. Nicholls, S. Chintawar, C. Schnell, J. P. Antel, N. D. Allen, M. Z. Cader, R. Wade-Martins, W. S. James and S. A. Cowley (2017). "A Highly Efficient Human Pluripotent Stem Cell Microglia Model Displays a Neuronal-Co-culture-Specific Expression Profile and Inflammatory Response." Stem Cell Reports **8**(6): 1727-1742.
22. Hall, C. J., R. H. Boyle, J. W. Astin, M. V. Flores, S. H. Oehlers, L. E. Sanderson, F. Ellett, G. J. Lieschke, K. E. Crosier and P. S. Crosier (2013). "Immunoresponsive gene 1 augments bactericidal activity of macrophage-lineage cells by regulating beta-oxidation-dependent mitochondrial ROS production." Cell Metab **18**(2): 265-278.
23. Hao, Y., S. Hao, E. Andersen-Nissen, W. M. Mauck, 3rd, S. Zheng, A. Butler, M. J. Lee, A. J. Wilk, C. Darby, M. Zager, P. Hoffman, M. Stoeckius, E. Papalexi, E. P. Mimitou, J. Jain, A. Srivastava, T. Stuart, L. M. Fleming, B. Yeung, A. J. Rogers, J. M. McElrath, C. A. Blish, R. Gottardo, P. Smibert and R. Satija (2021). "Integrated analysis of multimodal single-cell data." Cell **184**(13): 3573-3587 e3529.
24. Hinwood, M., R. J. Tynan, J. L. Charnley, S. B. Beynon, T. A. Day and F. R. Walker (2013). "Chronic stress induced remodeling of the prefrontal cortex: structural re-organization of microglia and the inhibitory effect of minocycline." Cereb Cortex **23**(8): 1784-1797.
25. Imamura, K., N. Hishikawa, M. Sawada, T. Nagatsu, M. Yoshida and Y. Hashizume (2003). "Distribution of major histocompatibility complex class II-positive microglia and cytokine profile of Parkinson's disease brains." Acta Neuropathol **106**(6): 518-526.
26. Kim, J. H., D. J. Choi, H. K. Jeong, J. Kim, D. W. Kim, S. Y. Choi, S. M. Park, Y. H. Suh, I. Jou and E. H. Joe (2013). "DJ-1 facilitates the interaction between STAT1 and its phosphatase, SHP-1, in brain microglia and astrocytes: A novel anti-inflammatory function of DJ-1." Neurobiol Dis **60**: 1-10.

27. Kim, R. H., P. D. Smith, H. Aleyasin, S. Hayley, M. P. Mount, S. Pownall, A. Wakeham, A. J. You-Ten, S. K. Kalia, P. Horne, D. Westaway, A. M. Lozano, H. Anisman, D. S. Park and T. W. Mak (2005). "Hypersensitivity of DJ-1-deficient mice to 1-methyl-4-phenyl-1,2,3,6-tetrahydropyrindine (MPTP) and oxidative stress." Proc Natl Acad Sci U S A **102**(14): 5215-5220.
28. Krebiehl, G., S. Ruckerbauer, L. F. Burbulla, N. Kieper, B. Maurer, J. Waak, H. Wolburg, Z. Gizatullina, F. N. Gellerich, D. Woitalla, O. Riess, P. J. Kahle, T. Proikas-Cezanne and R. Kruger (2010). "Reduced basal autophagy and impaired mitochondrial dynamics due to loss of Parkinson's disease-associated protein DJ-1." PLoS One **5**(2): e9367.
29. Lavisse, S., S. Goutal, C. Wimberley, M. Tonietto, M. Bottlaender, P. Gervais, B. Kuhnast, M. A. Peyronneau, O. Barret, J. Lagarde, M. Sarazin, P. Hantraye, C. Thiriez and P. Remy (2021). "Increased microglial activation in patients with Parkinson disease using [(18)F]-DPA714 TSPO PET imaging." Parkinsonism Relat Disord **82**: 29-36.
30. Liao, Y., G. K. Smyth and W. Shi (2019). "The R package Rsubread is easier, faster, cheaper and better for alignment and quantification of RNA sequencing reads." Nucleic Acids Res **47**(8): e47.
31. Lin, Z., C. Chen, D. Yang, J. Ding, G. Wang and H. Ren (2021). "DJ-1 inhibits microglial activation and protects dopaminergic neurons in vitro and in vivo through interacting with microglial p65." Cell Death Dis **12**(8): 715.
32. Lind-Holm Mogensen, F., A. Scafidi, A. Poli and A. Michelucci (2023). "PARK7/DJ-1 in microglia: implications in Parkinson's disease and relevance as a therapeutic target." J Neuroinflammation **20**(1): 95.
33. Love, M. I., W. Huber and S. Anders (2014). "Moderated estimation of fold change and dispersion for RNA-seq data with DESeq2." Genome Biol **15**(12): 550.
34. Lun, A. T. L., S. Riesenfeld, T. Andrews, T. P. Dao, T. Gomes, J. participants in the 1st Human Cell Atlas and J. C. Marioni (2019). "EmptyDrops: distinguishing cells from empty droplets in droplet-based single-cell RNA sequencing data." Genome Biol **20**(1): 63.
35. Martin, M. (2011). "Cutadapt removes adapter sequences from high-throughput sequencing reads." EMBnet.journal **17**(1): 10-12.
36. Meiser, J., S. Delcambre, A. Wegner, C. Jager, J. Ghelfi, A. F. d'Herouel, X. Dong, D. Weindl, C. Stautner, Y. Nonnenmacher, A. Michelucci, O. Popp, F. Giesert, S. Schildknecht, L. Kramer, J. G. Schneider, D. Woitalla, W. Wurst, A. Skupin, D. M. Weisenhorn, R. Kruger, M. Leist and K. Hiller (2016). "Loss of DJ-1 impairs antioxidant response by altered glutamine and serine metabolism." Neurobiol Dis **89**: 112-125.
37. Michelucci, A., T. Cordes, J. Ghelfi, A. Pailot, N. Reiling, O. Goldmann, T. Binz, A. Wegner, A. Tallam, A. Rausell, M. Buttini, C. L. Linster, E. Medina, R. Balling and K. Hiller (2013). "Immune-responsive gene 1 protein links metabolism to immunity by catalyzing itaconic acid production." Proc Natl Acad Sci U S A **110**(19): 7820-7825.
38. Molder, F., K. P. Jablonski, B. Letcher, M. B. Hall, C. H. Tomkins-Tinch, V. Sochat, J. Forster, S. Lee, S. O. Twardziok, A. Kanitz, A. Wilm, M. Holtgrewe, S. Rahmann, S. Nahnsen and J. Koster (2021).

"Sustainable data analysis with Snakemake." F1000Res **10**: 33.

39. Nielsen, H. H., J. Qiu, S. Friis, L. Wermuth and B. Ritz (2012). "Treatment for Helicobacter pylori infection and risk of Parkinson's disease in Denmark." Eur J Neurol **19**(6): 864-869.
40. Pakpoor, J., A. Noyce, R. Goldacre, M. Selkihova, S. Mullin, A. Schrag, A. Lees and M. Goldacre (2017). "Viral hepatitis and Parkinson disease: A national record-linkage study." Neurology **88**(17): 1630-1633.
41. Paolicelli, R. C., A. Sierra, B. Stevens, M. E. Tremblay, A. Aguzzi, B. Ajami, I. Amit, E. Audinat, I. Bechmann, M. Bennett, F. Bennett, A. Bessis, K. Biber, S. Bilbo, M. Blurton-Jones, E. Boddeke, D. Brites, B. Brone, G. C. Brown, O. Butovsky, M. J. Carson, B. Castellano, M. Colonna, S. A. Cowley, C. Cunningham, D. Davalos, P. L. De Jager, B. de Strooper, A. Denes, B. J. L. Eggen, U. Eyo, E. Galea, S. Garel, F. Ginhoux, C. K. Glass, O. Gokce, D. Gomez-Nicola, B. Gonzalez, S. Gordon, M. B. Graeber, A. D. Greenhalgh, P. Gressens, M. Greter, D. H. Gutmann, C. Haass, M. T. Heneka, F. L. Heppner, S. Hong, D. A. Hume, S. Jung, H. Kettenmann, J. Kipnis, R. Koyama, G. Lemke, M. Lynch, A. Majewska, M. Malcangio, T. Malm, R. Mancuso, T. Masuda, M. Matteoli, B. W. McColl, V. E. Miron, A. V. Molofsky, M. Monje, E. Mracsko, A. Nadjar, J. J. Neher, U. Neniskyte, H. Neumann, M. Noda, B. Peng, F. Peri, V. H. Perry, P. G. Popovich, C. Pridans, J. Priller, M. Prinz, D. Ragozzino, R. M. Ransohoff, M. W. Salter, A. Schaefer, D. P. Schafer, M. Schwartz, M. Simons, C. J. Smith, W. J. Streit, T. L. Tay, L. H. Tsai, A. Verkhratsky, R. von Bernhardi, H. Wake, V. Wittamer, S. A. Wolf, L. J. Wu and T. Wyss-Coray (2022). "Microglia states and nomenclature: A field at its crossroads." Neuron **110**(21): 3458-3483.
42. Patrick, K. L., S. L. Bell, C. G. Weindel and R. O. Watson (2019). "Exploring the "Multiple-Hit Hypothesis" of Neurodegenerative Disease: Bacterial Infection Comes Up to Bat." Front Cell Infect Microbiol **9**: 138.
43. Perez-Sala, D. and M. A. Pajares (2023). "Appraising the Role of Astrocytes as Suppliers of Neuronal Glutathione Precursors." Int J Mol Sci **24**(9).
44. Pham, T. T., F. Giesert, A. Rothig, T. Floss, M. Kallnik, K. Weindl, S. M. Holter, U. Ahting, H. Prokisch, L. Becker, T. Klopstock, M. Hrabe de Angelis, K. Beyer, K. Gorner, P. J. Kahle, D. M. Vogt Weisenhorn and W. Wurst (2010). "DJ-1-deficient mice show less TH-positive neurons in the ventral tegmental area and exhibit non-motoric behavioural impairments." Genes Brain Behav **9**(3): 305-317.
45. Sack, M. N. (2006). "Mitochondrial depolarization and the role of uncoupling proteins in ischemia tolerance." Cardiovasc Res **72**(2): 210-219.
46. Salamanca, L., N. Mechawar, K. K. Murai, R. Balling, D. S. Bouvier and A. Skupin (2019). "MIC-MAC: An automated pipeline for high-throughput characterization and classification of three-dimensional microglia morphologies in mouse and human postmortem brain samples." Glia **67**(8): 1496-1509.
47. Schubert, M., S. Lindgreen and L. Orlando (2016). "AdapterRemoval v2: rapid adapter trimming, identification, and read merging." BMC Res Notes **9**: 88.
48. Sheng, C., X. Heng, G. Zhang, R. Xiong, H. Li, S. Zhang and S. Chen (2013). "DJ-1 deficiency perturbs microtubule dynamics and impairs striatal neurite outgrowth." Neurobiol Aging **34**(2): 489-498.

49. Sherman, B. T., M. Hao, J. Qiu, X. Jiao, M. W. Baseler, H. C. Lane, T. Imamichi and W. Chang (2022). "DAVID: a web server for functional enrichment analysis and functional annotation of gene lists (2021 update)." Nucleic Acids Res **50**(W1): W216-W221.

50. Smajic, S., C. A. Prada-Medina, Z. Landoulsi, J. Ghelfi, S. Delcambre, C. Dietrich, J. Jarazo, J. Henck, S. Balachandran, S. Pachchek, C. M. Morris, P. Antony, B. Timmermann, S. Sauer, S. L. Pereira, J. C. Schwamborn, P. May, A. Grunewald and M. Spielmann (2022). "Single-cell sequencing of human midbrain reveals glial activation and a Parkinson-specific neuronal state." Brain **145**(3): 964-978.

51. Smeyne, R. J., A. J. Noyce, M. Byrne, R. Savica and C. Marras (2021). "Infection and Risk of Parkinson's Disease." J Parkinsons Dis **11**(1): 31-43.

52. Smith, K. L., M. S. Kassem, D. J. Clarke, M. P. Kuligowski, M. A. Bedoya-Perez, S. M. Todd, J. Lagopoulos, M. R. Bennett and J. C. Arnold (2019). "Microglial cell hyper-ramification and neuronal dendritic spine loss in the hippocampus and medial prefrontal cortex in a mouse model of PTSD." Brain Behav Immun **80**: 889-899.

53. Sonnenfeld, G., J. E. Cunnick, A. V. Armfield, P. G. Wood and B. S. Rabin (1992). "Stress-induced alterations in interferon production and class II histocompatibility antigen expression." Brain Behav Immun **6**(2): 170-178.

54. Sousa, C., A. Golebiewska, S. K. Poovathingal, T. Kaoma, Y. Pires-Afonso, S. Martina, D. Coowar, F. Azuaje, A. Skupin, R. Balling, K. Biber, S. P. Niclou and A. Michelucci (2018). "Single-cell transcriptomics reveals distinct inflammation-induced microglia signatures." EMBO Rep **19**(11).

55. Stirling, D. R., M. J. Swain-Bowden, A. M. Lucas, A. E. Carpenter, B. A. Cimini and A. Goodman (2021). "CellProfiler 4: improvements in speed, utility and usability." BMC Bioinformatics **22**(1): 433.

56. Tallam, A., T. M. Perumal, P. M. Antony, C. Jager, J. V. Fritz, L. Vallar, R. Balling, A. Del Sol and A. Michelucci (2016). "Gene Regulatory Network Inference of Immunoresponsive Gene 1 (IRG1) Identifies Interferon Regulatory Factor 1 (IRF1) as Its Transcriptional Regulator in Mammalian Macrophages." PLoS One **11**(2): e0149050.

57. Tansey, M. G., R. L. Wallings, M. C. Houser, M. K. Herrick, C. E. Keating and V. Joers (2022). "Inflammation and immune dysfunction in Parkinson disease." Nat Rev Immunol **22**(11): 657-673.

58. Team, R. C. (2021). "R: A language and environment for statistical computing. R Foundation for Statistical Computing, Vienna, Austria."

59. Terkelsen, M. H., I. H. Klaestrup, V. Hvingelby, J. Lauritsen, N. Pavese and M. Romero-Ramos (2022). "Neuroinflammation and Immune Changes in Prodromal Parkinson's Disease and Other Synucleinopathies." J Parkinsons Dis **12**(s1): S149-S163.

60. Toda, G., T. Yamauchi, T. Kadowaki and K. Ueki (2021). "Preparation and culture of bone marrow-derived macrophages from mice for functional analysis." STAR Protoc **2**(1): 100246.

61. Trudler, D., O. Weinreb, S. A. Mandel, M. B. Youdim and D. Frenkel (2014). "DJ-1 deficiency triggers microglia sensitivity to dopamine toward a pro-inflammatory phenotype that is attenuated by rasagiline." J Neurochem **129**(3): 434-447.

62. van Wilgenburg, B., C. Browne, J. Vowles and S. A. Cowley (2013). "Efficient, long term production of monocyte-derived macrophages from human pluripotent stem cells under partly-defined and fully-defined conditions." PLoS One **8**(8): e71098.
63. Vidal-Itriago, A., R. A. W. Radford, J. A. Aramideh, C. Maurel, N. M. Scherer, E. K. Don, A. Lee, R. S. Chung, M. B. Graeber and M. Morsch (2022). "Microglia morphophysiological diversity and its implications for the CNS." Front Immunol **13**: 997786.
64. Waak, J., S. S. Weber, A. Waldenmaier, K. Gorner, M. Alunni-Fabbroni, H. Schell, D. Vogt-Weisenhorn, T. T. Pham, V. Reumers, V. Baekelandt, W. Wurst and P. J. Kahle (2009). "Regulation of astrocyte inflammatory responses by the Parkinson's disease-associated gene DJ-1." FASEB J **23**(8): 2478-2489.
65. Wang, H., X. Liu, C. Tan, W. Zhou, J. Jiang, W. Peng, X. Zhou, L. Mo and L. Chen (2020). "Bacterial, viral, and fungal infection-related risk of Parkinson's disease: Meta-analysis of cohort and case-control studies." Brain Behav **10**(3): e01549.
66. Wang, Y., X. Kang, X. Kang and F. Yang (2023). "S100A6: molecular function and biomarker role." Biomark Res **11**(1): 78.
67. Zhang, Y., Y. Dong, Y. Zhu, D. Sun, S. Wang, J. Weng, Y. Zhu, W. Peng, B. Yu and Y. Jiang (2022). "Microglia-specific transcriptional repression of interferon-regulated genes after prolonged stress in mice." Neurobiol Stress **21**: 100495.

Figures

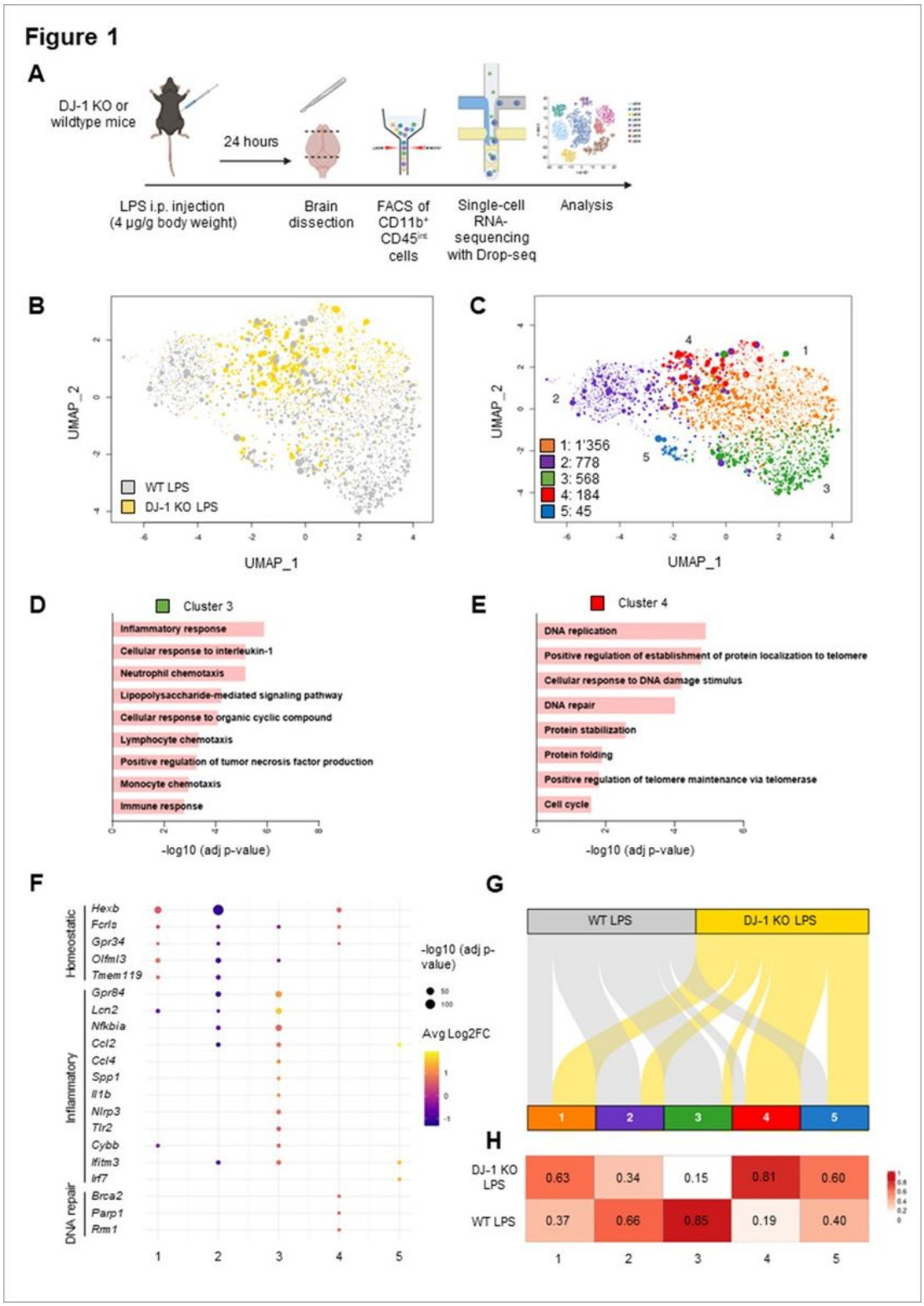

Figure 1

Subset of classical activated microglia is mainly composed of cells originated from wildtype mice 24 hours after systemic LPS-induced inflammation. A) Schematic representation of scRNA-sequencing analyses of CD11b^{+}CD45^{int} microglial cells isolated either from PARK7/DJ-1 KO or wildtype mice 24h following LPS treatment. **B)** UMAP showing 2'931 CD11b^{+}CD45^{int} microglial cells from PARK7/DJ-1 KO (yellow) and wildtype (grey) mice 24h after LPS treatment (n = 2 mice per group). **C)** UMAP showing

clustering analysis of 2’931 single microglial cells. Numbers indicate amount of cells per cluster. **D-E)** Gene ontology terms corresponding to upregulated genes (adjusted p-value < 0.05, log2FC ≥ 0.5) comparing **(D)** Cluster 3 or **(E)** Cluster 4 to the other clusters. **F)** Dot plot showing selected differentially expressed genes (adjusted p-value < 0.05, |log2FC| ≥ 0.5) characterizing each cluster. Color code represents the average log2FC, while the size of the dot is proportional to the statistical significance indicated as –log10 (adjusted p-value). **G)** Alluvial plot showing $CD11b^{+}CD45^{int}$ microglial cells flowing into the identified 5 normalized clusters according to their origin, either from wildtype (grey) or PARK7/DJ-1 KO (yellow) mice. **H)** Heatmap showing percentages of cells deriving either from PARK7/DJ-1 KO or wildtype mice.

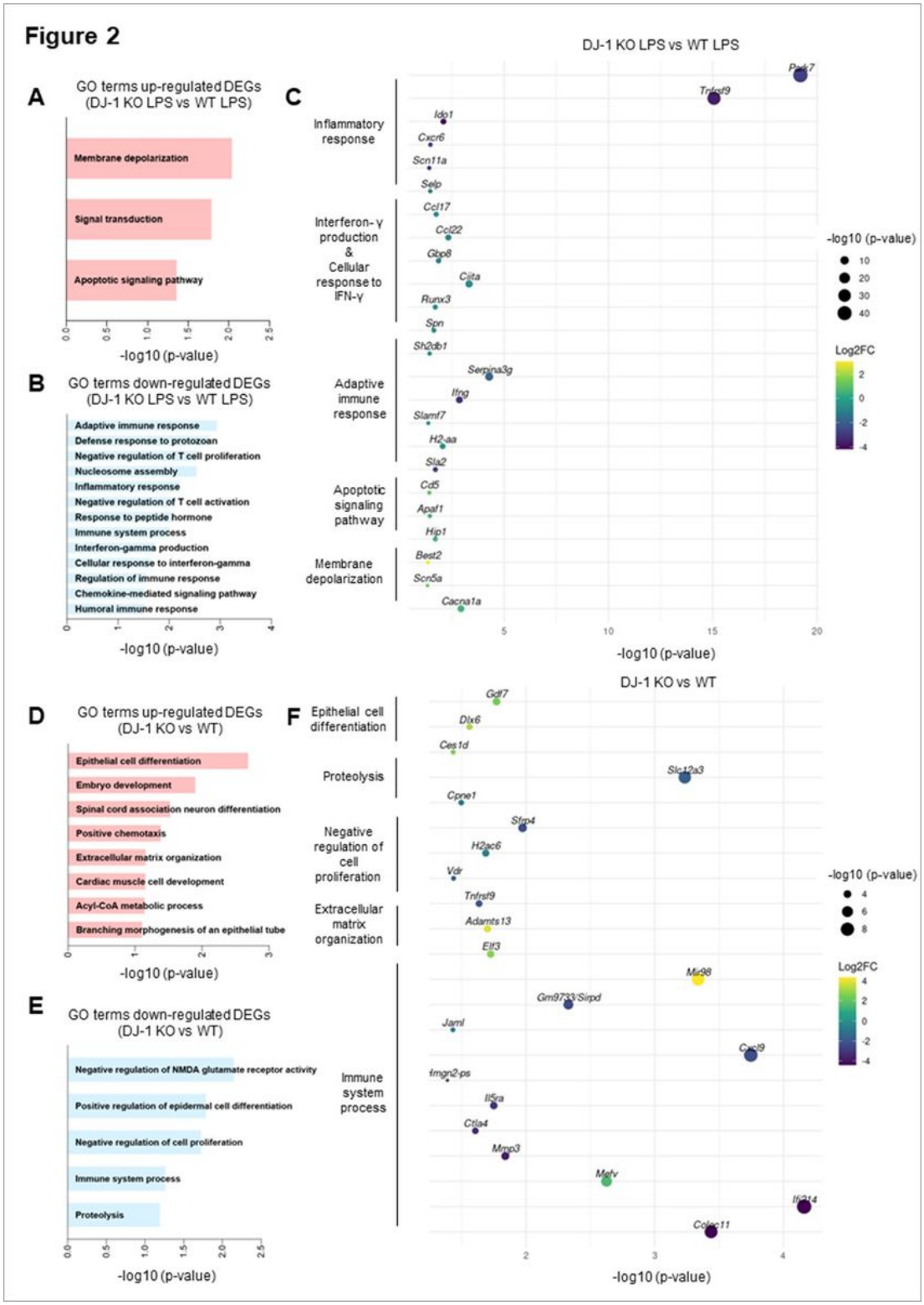

Figure 2

Distinct reaction of microglia in PARK7/DJ-1 KO mice compared to wildtype mice 6 hours after systemic LPS-induced inflammation and at baseline. A-B) GO terms corresponding to **(A)** upregulated or **(B)** downregulated genes comparing microglia in PARK7/DJ-1 KO and wildtype mice 6h after LPS treatment. **C)** Dot plot showing a selection of top 50 differentially expressed genes (p-value < 0.05, |log2FC| ≥ 0.5) comparing CD11b^{+} microglia isolated from PARK7/DJ-1 KO and wildtype mice 6h after LPS-induced

inflammation. **D-E)** GO terms corresponding to **(D)** upregulated or **(E)** downregulated genes comparing microglia in PARK7/DJ-1 KO and wildtype mice at baseline. **F)** Dot plot showing top 50 most variable genes (p-value < 0.05, |log2FC| ≥ 0.5) comparing CD11b^{+} microglia isolated from PARK7/DJ-1 KO and wildtype mice at baseline.

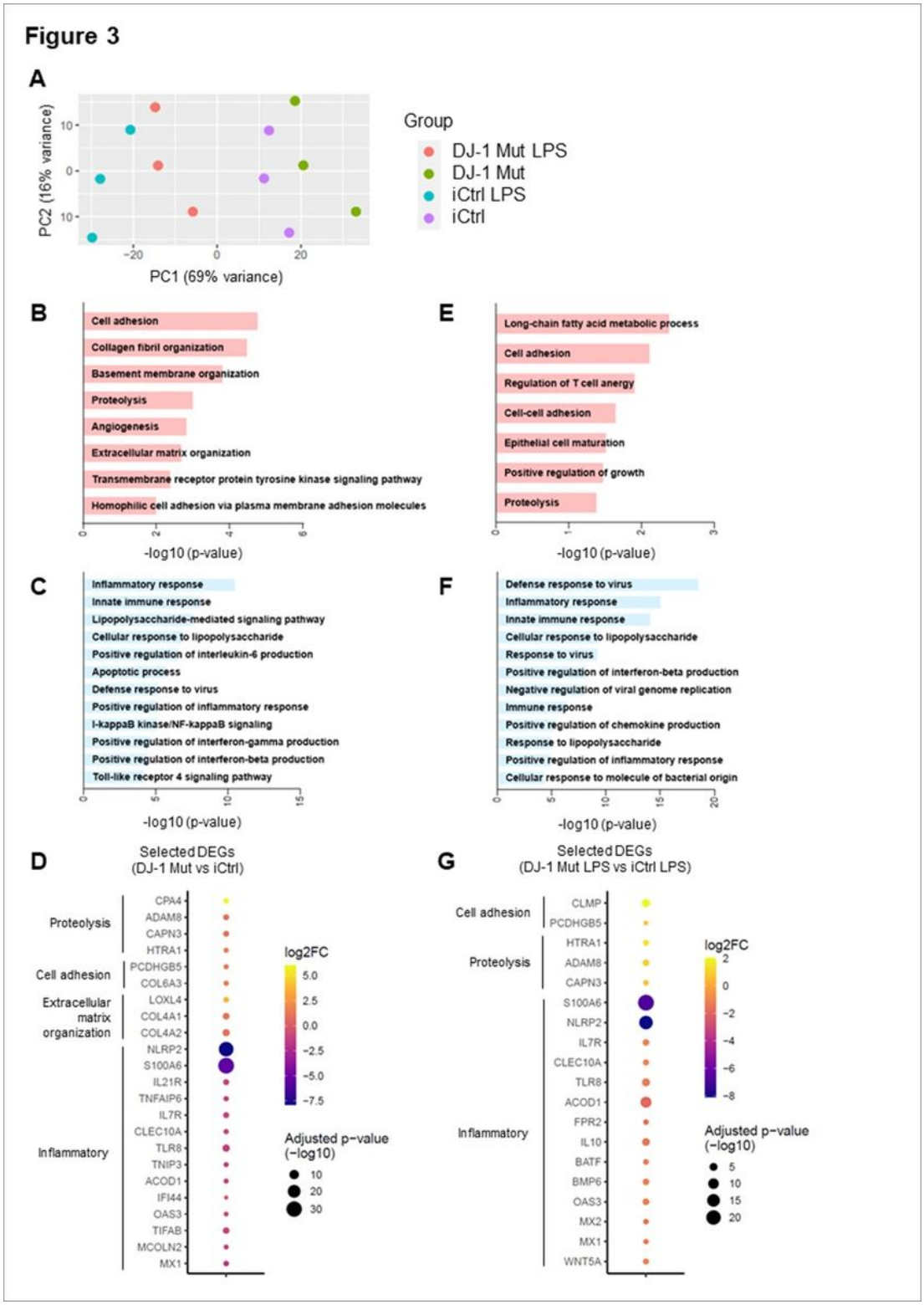

Figure 3

Discrete iPSC-derived microglia signatures between PARK7/DJ-1 mutant and isogenic control cells under LPS treatment and at baseline. A) Design aware Principal component analysis (PCA) plot showing clustering of 3 replicates of differentiated iPSC-derived microglia (iMG) per condition: PARK7/DJ-1 mutant and isogenic control iMG untreated or treated with LPSfor 6h. **B-C)**GO terms corresponding to **(B)**upregulated or **(C)** downregulated genes comparing PARK7/DJ-1 mutant and isogenic control iMG at baseline. **D)** Dot plot showing selected differentially expressed genes (adjusted p-value < 0.05, |log2FC| ≥ 0.5) comparing PARK7/DJ-1 mutant and isogenic control iMGat baseline. **E-F)** GO terms corresponding to **(E)** upregulated or **(F)** downregulated genes comparing PARK7/DJ-1 mutant and isogenic control iMG after 6h LPS treatment. **G)** Dot plot showing selected differentially expressed genes (adjusted p-value < 0.05, |log2FC| ≥ 0.5) comparing PARK7/DJ-1 mutant and isogenic control iMGafter treatment with LPS for 6h.

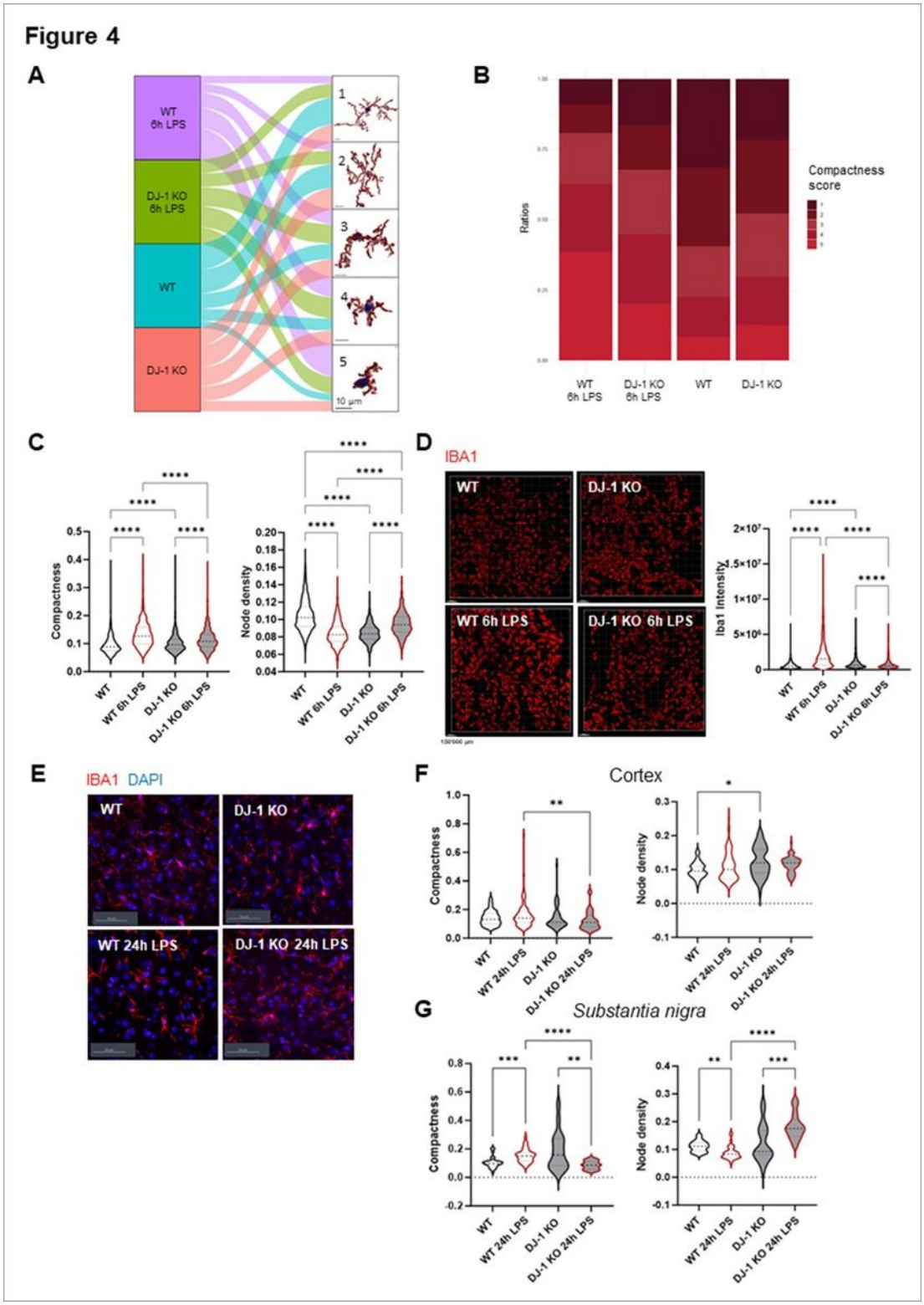

Figure 4

Microglia in PARK7/DJ-1 KO mice show a more compact morphology compared to wildtype mice at baseline and a less amoeboid morphology 6 and 24 hours after LPS treatment. A) Alluvial plot showing MIC-MAC analysis of IBA1^{+} cortical microglial cells flowing into 5 morphological clusters (pictures show 3D reconstructions of a representative microglial cell per cluster, scale bar: 10 µm) based on compactness score (spanning from cluster 1, corresponding to homeostatic ramified microglia, to cluster

5, representing activated amoeboid cells) according to their mouse origin, either from wildtype (baseline in purple, 6h LPS in turquoise) or PARK7/DJ-1 KO (baseline in red, 6h LPS in green) (n = 3-4 mice). **B)** Bar graph showing the ratios of the identified clusters across the four different conditions (wildtype or PARK7/DJ-1 KO 6h LPS, wildtype or PARK7/DJ-1 KO baseline) (mean = 244 ± 19 cells per cortex region from 3-4 mice per group). Color bar shows compactness score. **C)** Violin plots showing mean compactness (left) or node density (right) (dotted line) of cortical microglial cells in wildtype or PARK7/DJ-1 KO mice with or without 6h LPS treatment. Kruskal-Wallis test with Dunn's test for multiple comparisons. ****p<0.00005 (mean = 244 ± 19 cells per cortex region from 3-4 mice per group). **D)** Left: representative pictures showing intensity of cortical $IBA1^+$ cells in PARK7/DJ-1 KO or wildtype mice with or without 6h LPS treatment. Scale bar: 150'000 µm. Right: violin plots showing mean of IBA1 intensity (dotted line) of cortical microglial cells in wildtype or PARK7/DJ-1 KO mice with or without 6h LPS treatment. Kruskal-Wallis test with Dunn's test for multiple comparisons. ****p<0.00005 (mean = 244 ± 19 cells per cortex region from 3-4 mice per group). **E)** Representative pictures showing cortical $IBA1^+$ cells in PARK7/DJ-1 KO or wildtype mice with or without 24h LPS treatment. Scale bar: 50 µm. **F)** Violin plots showing mean compactness (left) or node density (right) (dotted line) of cortical microglial cells in wildtype or PARK7/DJ-1 KO mice with or without 24h LPS treatment. Kruskal-Wallis test with Dunn's test for multiple comparisons. **p<0.01, *p<0.05 (mean = 22 ± 2 cells per cortex region from 3 mice per group). **G)** Violin plots showing mean compactness (left) or node density (right) (dotted line) of substantia nigra microglial cells in wildtype or PARK7/DJ-1 KO mice with or without 24h LPS treatment. Kruskal-Wallis test with Dunn's test for multiple comparisons. ****p<0.00005, ***p<0.005, **p<0.01 (mean = 9 ± 1 cells per substantia nigra region from 3 mice per group).

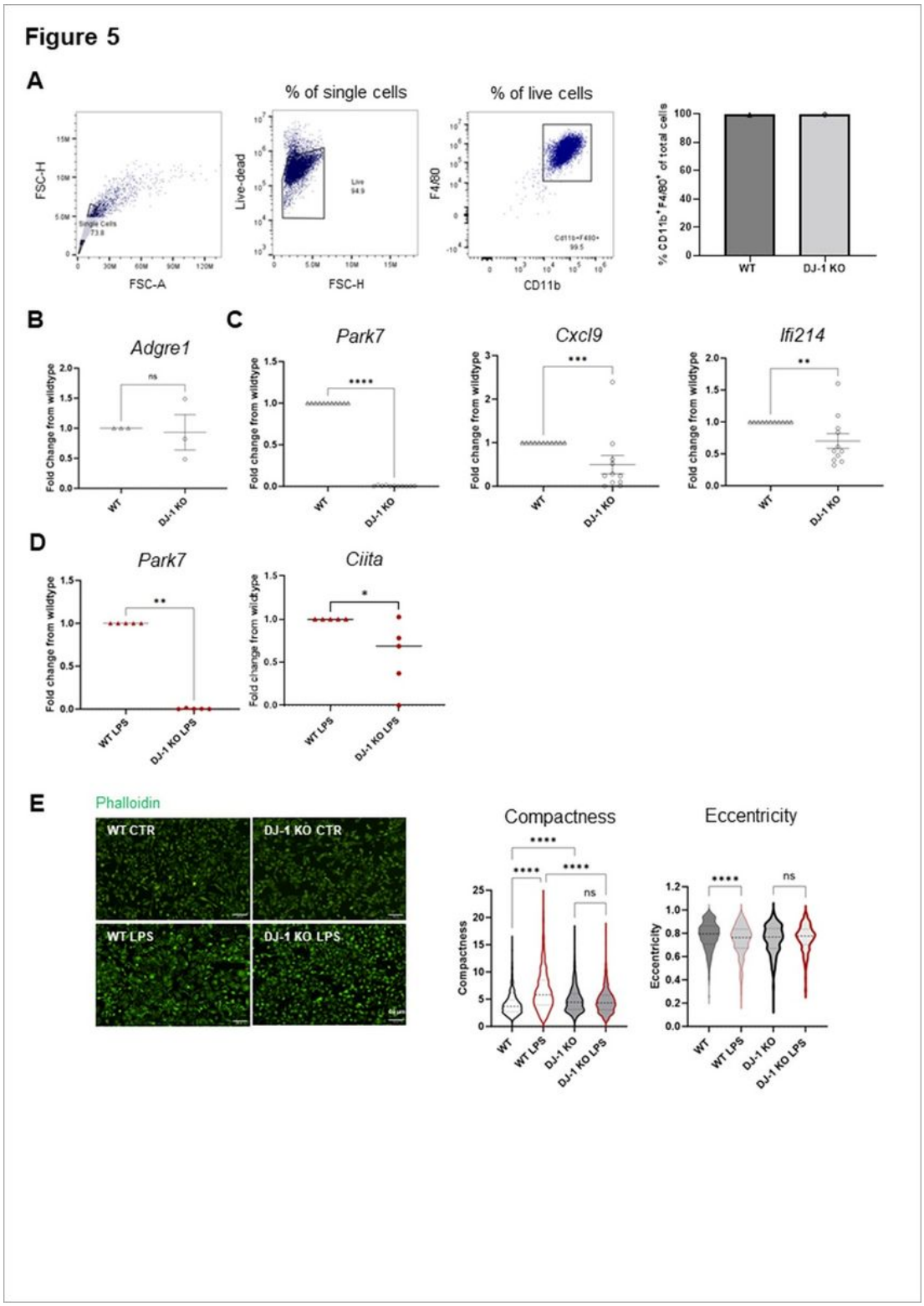

Figure 5

Characterization of *PARK7*/DJ-1-deficient bone marrow-derived macrophages at baseline and after LPS-treatment

A) Gating strategy used to measure percentages of $CD11b^{+}F4/80^{+}$ BMDMs among total cells (left) and corresponding quantification (n = 1 mouse per group) (right). **B)** Gene expression levels of *Adgre1* (F4/80)

comparing BMDMs originating from wildtype and *PARK7*/DJ-1 KO mice analyzed by qPCR. Graph shows mean of fold change (wildtype condition set at 1; *Gapdh* as housekeeping gene) ± SEM. Mann-Whitney test, ns: not significant (n = 3 mice per group). **C)** Gene expression levels of *Park7, Cxcl9* and *Ifi214* in wildtype and *PARK7*/DJ-1 KO BMDMs analyzed by qPCR. Graphs represent mean of fold change (wildtype condition set at 1; *Gapdh* as housekeeping gene) ± SEM. Mann-Whitney test, *p<0.05; ****p<0.00005, ***p<0.001 (n = 10 mice per group). **D)** Gene expression levels of *Park7* and *Ciita* in wildtype and *PARK7*/DJ-1 KO BMDMs under 6h LPS (100 ng/mL) treatment analyzed by qPCR. Graphs represent mean of fold change (wildtype condition set at 1; *Gapdh* as housekeeping gene) ± SEM. Mann-Whitney test, **p<0.01, *p<0.05; (n = 5 mice per group). **E)** Representative pictures of wildtype and *PARK7*/DJ-1 KO BMDMs stained with phalloidin showing actin filaments with and without 6h LPS (100 ng/mL) treatment (left) and corresponding quantification of compactness and eccentricity scores (right). Scale bar: 69 µm. Kruskal-Wallis test for multiple comparisons. ****p<0.00005, ns: not significant (n = 3 mice per group).

Supplementary Files

This is a list of supplementary files associated with this preprint. Click to download.

- SupplementaryFiguresFLM.pdf
- TableS1FLM.docx
- TableS2FLM.docx
- TableS3FLM.docx
- TableS4FLM.xlsx
- TableS5FLM.xlsx
- TableS6FLM.xlsx